North Anatolian Fault in the Gulf of Izmit (Turkey): Rapid vertical motion in response to minor bends of a nonvertical continental transform

Marie-Helene Cormier,[1] Leonardo Seeber,[1] Cecilia M. G. McHugh,[1] Alina Polonia,[2] Namik Çagatay,[3] Ömer Emre,[4] Luca Gasperini,[2] Naci Görür,[3] Giovanni Bortoluzzi,[2] Enrico Bonatti,[2] William B. F. Ryan,[1] and Kori R. Newman[1]

Received 18 January 2005; revised 14 December 2005; accepted 27 December 2005; published 25 April 2006.

[1] The catastrophic rupture of the North Anatolian Fault east of the Marmara Sea on 17 August 1999 highlighted a need for mapping the underwater extension of that continental transform. A new bathymetric map of Izmit Gulf indicates that the fault follows the axis of the gulf with a few minor bends. Submerged shorelines and shelf breaks that formed during the Last Glacial Maximum provide markers to quantify vertical deformation. Variable tilting of these horizons reveals that vertical deformation is highest just south of the fault. A correlation between vertical deformation of the southern fault block and distance to fault bends can be accounted for by a fault dipping steeply to the south. Hence subsidence (uplift) of the southern, hanging wall block would be expected where the fault strikes at a slightly transtensional (transpressional) orientation to relative plate motion. Subsidence reaches about 8 mm/yr west of the town of Golcuk and might be accommodated in 1–2 m subsidence events during large earthquakes. That scenario is compatible with the tsunami runups and the coseismic subsidence of the southern shore that occurred in 1999. Seafloor morphology also suggests that earthquakes are accompanied by widespread gas and fluid release. The periphery of the deepest basin displays a hummocky texture diagnostic of sediment fluidization, and mud volcanoes occur west of Hersek peninsula that might be activated by earthquakes. Finally, the backscatter imagery reveals a series of lineaments midway through the gulf that are interpreted as products of the 1999 surface rupture. The seafloor is undisturbed farther west, suggesting that surface slip decreased to an insignificant level beyond Hersek. Possibly, the stress shadow from the 10 July 1894 earthquake, which was felt strongly along the western Izmit Gulf, contributed to arrest the 1999 surface rupture.

Citation: Cormier, M.-H., et al. (2006), North Anatolian Fault in the Gulf of Izmit (Turkey): Rapid vertical motion in response to minor bends of a nonvertical continental transform, *J. Geophys. Res.*, *111*, B04102, doi:10.1029/2005JB003633.

1. Introduction

[2] The 1600-km-long right-lateral North Anatolian Fault has been rupturing across Turkey from east to west in a series of large earthquakes during the 20th century [*Toksöz et al.*, 1979; *Barka*, 1996; *Stein et al.*, 1997]. That rupture front advanced 160 km in 1999 in two disastrous earthquakes (Mw = 7.5 and 7.2) and the next earthquake is expected to rupture beneath the Marmara Sea [*Barka*, 1999; *Hubert-Ferrari et al.*, 2000; *Parsons et al.*, 2000; *Reilinger et al.*, 2000b]. Because this region is home to about 20 million people and much of the country's industrial activity, seismic hazards are particularly high. The Turkish authorities thus coordinated a large international effort to fully characterize the submerged portion of the North Anatolian Fault [*Görür et al.*, 2002]. As part of that effort, a joint Italian, Turkish, and American project focused on key portions of the Marmara Sea shelves during two expeditions in fall 2000 and spring 2001 [*Polonia et al.*, 2002]. This paper analyzes some of the high-resolution bathymetry data collected during these two surveys.

[3] The northern branch of the North Anatolian Fault enters the eastern Marmara Sea through the Gulf of Izmit, a 50-km-long EW oriented coastal inlet [*Sengör et al.*, 1985; *Barka and Kadinsky-Cade*, 1988; *Wong et al.*, 1995; *Görür et al.*, 1997; *Kusçu et al.*, 2002] (Figure 1). The Gulf of Izmit comprises three basins: the western basin, the central basin, and the eastern basin (also known as the Darica basin, Karamürsel basin, and Golcuk or Izmit basin, respectively).

[1] Lamont-Doherty Earth Observatory of Columbia University, Palisades, New York, USA.
[2] Institute of Marine Sciences, Consiglio Nazionale delle Richerche, Bologna, Italy.
[3] Istanbul Technical University, Istanbul, Turkey.
[4] General Directorate of Mineral Research and Exploration, Ankara, Turkey.

0148-0227/06/2005JB003633$09.00

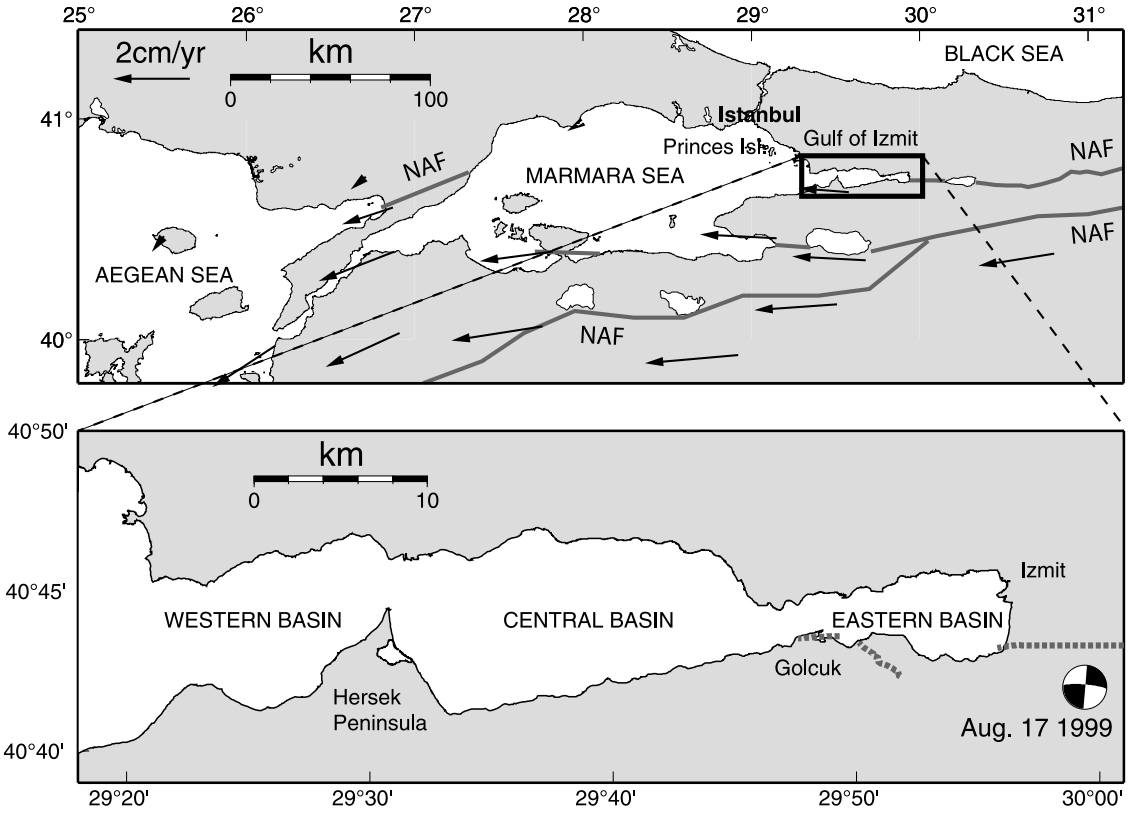

Figure 1. (top) Regional setting of the Marmara Sea, with the northern and southern branches of the North Anatolian Fault (NAF). Arrows indicate GPS velocities relative to a stable Eurasia [*McClusky et al.*, 2000]. (bottom) Area of the Gulf of Izmit. Dashed line indicates the land rupture from the 17 August 1999 earthquake [*Barka et al.*, 2002; *Emre et al.*, 2003a]. Fault plane solution is from the Harvard catalogue.

Each basin is 10–20 km long, 5–9 km wide, and 40–210 m deep. They are separated by two shallow sills located north of Hersek peninsula (54 m deep) and north of Golcuk (33 m deep). Prior to the acquisition of high-resolution bathymetric data, the geometry of the North Anatolian Fault in that area was inferred from conventional bathymetry, coastal morphology, grids of seismic profiles, and seismicity [*Barka and Kusçu*, 1996; *Alpar*, 1999; *Gökasan et al.*, 2001; *Alpar and Yaltirak*, 2002; *Kusçu et al.*, 2002]. Seismic surveys in particular revealed that the shallow subsurface is affected by a series of active faults and that strata are generally tilted and folded. However, because the spacing of these profiles range from a few 100 m to a few km, the interpretation of the fault trends remained open to debate.

[4] The present study reveals several unexpected results that can be summarized as follow. First, the high-resolution bathymetry highlights the trace of a major fault strand through Izmit Bay that is more linear than previously thought. Minor faults correspond to either surficial en echelon Riedel shears forming above that main strand, or are associated with sediment fluidization structures. Second, vertical motion is highly asymmetric about the fault, with rapid deformation affecting the southern fault block, and a relatively stable northern fault block. Lastly, surface slip from the 1999 earthquake arrested or tailed off abruptly halfway through Izmit Gulf rather than propagating another 30 km westward, as was suggested from the analysis of other geophysical data. These results are detailed below and a model is proposed that can account for them.

2. Data Acquisition and Processing

[5] Complete multibeam bathymetric coverage of the western and central basins was collected in 2000 and 20001 to characterize the plan view geometry of active fault segments. High-resolution seismic (chirp) profiles were acquired concurrently to image shallow fault structures (<20 m beneath seafloor). The bathymetric maps in Figures 2a and 2b compile data collected with three different multibeam systems. Most of the area west of the Hersek peninsula was surveyed during expedition MARMARA2000 of the *R/V Odin Finder* with two multibeam systems, the Simrad EM300 (30 kHz) and EM3000 (300 kHz). The remaining area was surveyed during expedition MARMARA2001 of the *R/V Urania* with a portable SeaBeam1180 (180 kHz) multibeam. All three systems provide a vertical resolution better than 10 cm and a mean footprint of a few square meters over the shelf. The bathymetry and backscatter data set was processed with the open source software MB-System [*Caress and Chayes*, 2002]. Precise navigation relied on differential GPS positioning and bathymetric maps are referenced to the WGS84 datum. Because the ships could not survey safely and efficiently in waters shallower than 20–30 m, the existence of subsidiary faults branches very close to shore cannot be ascertained from this study.

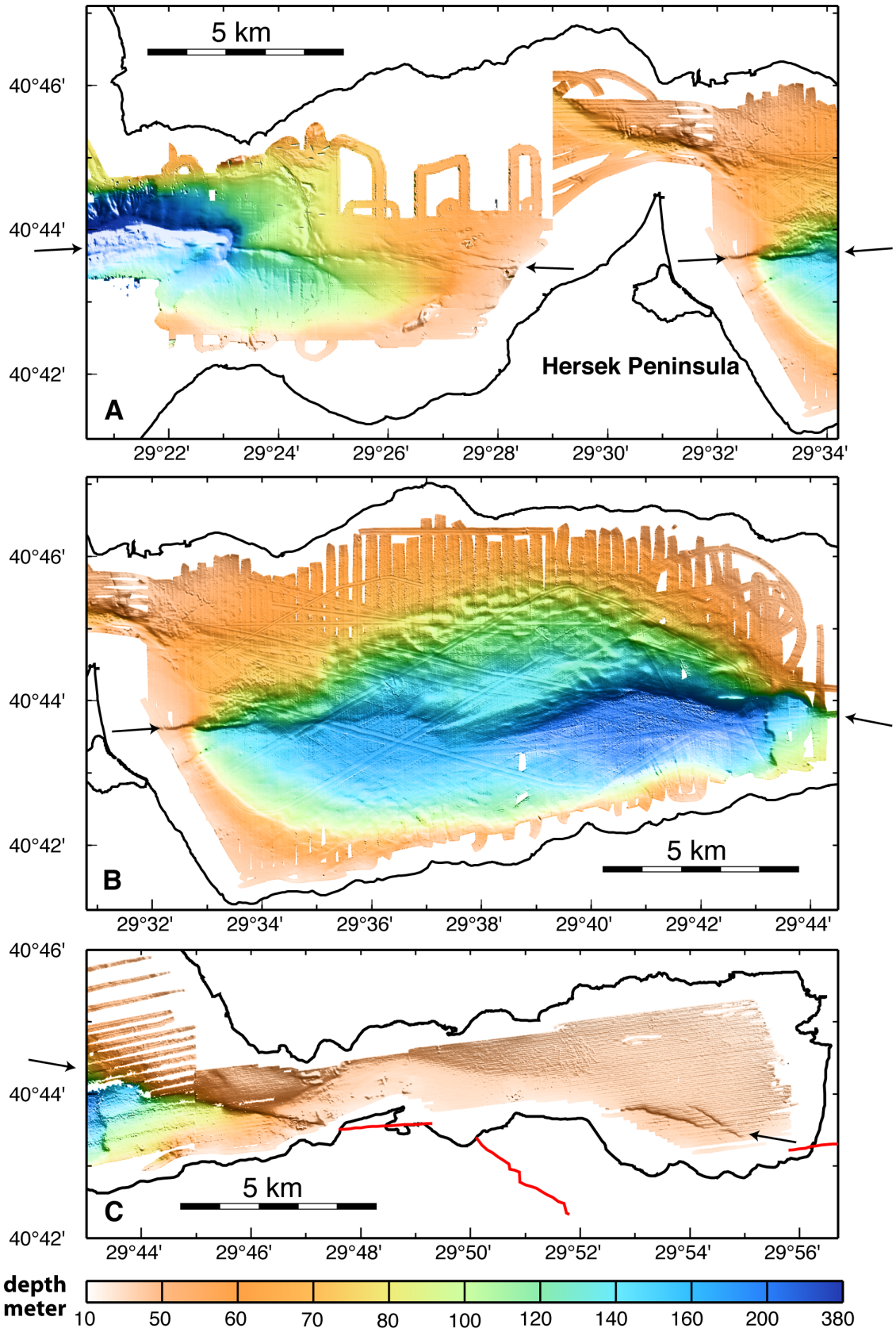

Figure 2. Multibeam bathymetry of Izmit Gulf: (a) western basin, (b) central basin, and (c) eastern basin. Artificial sun illumination is from the northeast. Arrows point to segments of the North Anatolian Fault. Figures 2a and 2b combine data from expeditions MARMARA2000 and MARMARA2001, and Figure 2c displays data provided by SHOD (see section 2).

[6] The shallow water depths prevailing in Izmit Bay required that survey lines be spaced 50–250 m apart to ensure continuous bathymetry coverage. The chirp subbottom profiles acquired along the same survey tracks thus provide tight control on the shallow subsurface structures. Most chirp profiles across the shelves reveal an acoustically transparent layer draping over a reflective acoustic basement. Where chirp profiles penetrate beneath the acoustic basement, they indicate a discordant, erosional contact with the overlying transparent layer. Gravity cores collected in Izmit Gulf during the two surveys document that this transparent layer corresponds to a Holocene mud drape, and the underlying strong reflector acoustic basement to the subaerial erosion surface that formed during the last sea level lowstand [*Çagatay et al.*, 2003; *Polonia et al.*, 2004], a result consistent with other studies [*Aksu et al.*, 1999; *Kusçu et al.*, 2002]. The thickness of the Holocene drape varies from less than 1 m to more than 20 m, with vertical separations across fault strands systematically larger at the base of the Holocene than at the seafloor [*Kusçu et al.*, 2002; *Polonia et al.*, 2002]. Syntectonic sedimentation is not the only factor that controls thickness variations. Strong bottom currents in the Gulf of Izmit [*Algan et al.*, 1999] most likely redistribute Holocene sediments and contribute to subdue the tectonic fabric. Shallow sediments are also commonly gas charged, which can make it difficult to precisely map the base of the Holocene drape.

[7] Only sparse bathymetric coverage was produced during both expeditions east of 29°44′E, where the seafloor is largely shallower than 50 m. The multibeam bathymetry data displayed in Figure 2c were acquired in fall 1999 by the Turkish Department of Navigation, Hydrography and Oceanography (SHOD) and kindly made available for this study.

3. Physiography of Izmit Gulf and Surficial Fault Geometry

[8] The trace of an active fault that follows the approximate axis of the Western and Central basins is clearly visible in the multibeam bathymetry data (Figures 2, 3, and 4). Overall, the fault is continuous through these two basins, describing three small bends. The orientations of the fault segments defined by these bends are all compatible with that of the present N094°E ± 10° relative motion vector derived from GPS measurements across Izmit Gulf [*McClusky et al.*, 2000]. At a very local scale, the fault displays en echelon geometries typical of right-lateral transform faults, with individual steps just a few hundred meters across. Hence plate motion in western and central basins seems to be taken up on a single throughgoing fault. In particular, there is no evidence for major fault step overs and associated normal faults that could account for these basins. In contrast, eastern basin appears to be a small pull-apart basin accommodating a 1 km right step of the fault. A detailed description of the fault geometry through each of the three basins follows, with special emphasis on those features that permit to quantify fault-related deformation.

3.1. Western Basin

3.1.1. Fault Geometry

[9] The western (Darica) basin connects westward with the 1200-m-deep Çinarcik basin in the Marmara Sea via a narrow EW canyon (Figures 2a and 3a). The trace of the North Anatolian Fault follows the south wall of the canyon and offsets it right laterally by about 100m at 29°23.5′E, where the canyon bends to the south [*Polonia et al.*, 2004]. The fault strikes N094°E overall, but near 29°24.5′E, a splay deviates at N120°E toward the southeast and Hersek peninsula. Transform motion is divided between the two splays, as documented from a paleochannel detected beneath the thin Holocene cover that is offset right laterally across each splay [*Polonia et al.*, 2004]. Most of the right-lateral slip (∼90%) is accommodated on the main northern branch. East of the splay, the northern branch broadens into a series of en echelon left stepping segments. This geometry is compatible with that of Reidel shear fractures expected to develop along right-lateral transform faults [*Tchalenko*, 1970; *Sylvester*, 1988]. Each segment is 1–2 km long, strikes ∼N104°E (10° clockwise from the main fault orientation), and displays a small vertical separation (down to the south). The SE striking splay shares the same left stepping en echelon geometry. East of 29°27′E, that splay bends into a more EW direction. The main branch and the fault splay may meet again onto Hersek peninsula, or possibly a short distance east of the peninsula. Together, they define a lens 8–12 km long and about 1 km wide.

3.1.2. Variable Holocene Drape

[10] The smooth, low relief of the basin probably reflects the combined effect of bottom currents and high sedimentation rates. An isopach map of Holocene sediments derived from the chirp profiles indicates highly variable thicknesses across the basin (Figure 5). The relief of the erosional surface that underlies the Holocene mud is more pronounced than the bathymetry, with fault segments displaying higher vertical offset across steeper, south facing escarpments [*Kusçu et al.*, 2002; *Polonia et al.*, 2002]. The corrugated texture of the seafloor along the northern shore (Figure 2a) reflects the outcropping of stratigraphic layers. Hard substrate in that area is also suggested by the acoustically reflective bottom (Figure 4). Prevailing bottom currents are directed westward along the northern shore [*Algan et al.*, 1999] and may account for the low sediment deposition. In contrast, the thickness of the Holocene cover exceeds 20 m beneath the shallow depression south of the main fault and its splay (Figure 5).

3.1.3. Submerged Shoreline

[11] A striking feature of the basin is a west facing escarpment that extends north of the main fault at ∼29°24.5′E (Figures 2a and 6). This escarpment is bare of Holocene cover, as reflected by its acoustically reflective character (Figure 4), the rough seafloor texture near it, and the chirp records (Figure 5a). Nondeposition across the 3-km-long, 5–10-m-high feature may reflect the tendency for bottom currents to winnow sediments across topographic relief. The base of the escarpment is 90–95 m deep, roughly 5 m deeper than another contour parallel, sparsely sedimented incline mapped southwest of Istanbul during the same expedition (Figure 7). On the basis of their morphologies and nearly constant depths, we interpret both features as marking an ancient shoreline that formed around the perimeter of the Marmara Sea during the Last Glacial Maximum (LGM). Indeed, the Dardanelles Strait was the sill for a "Marmara Lake" that topped off at 85–95 mbsl during the last sea level lowstand [*Smith et al.*, 1995; *Ryan et al.*,

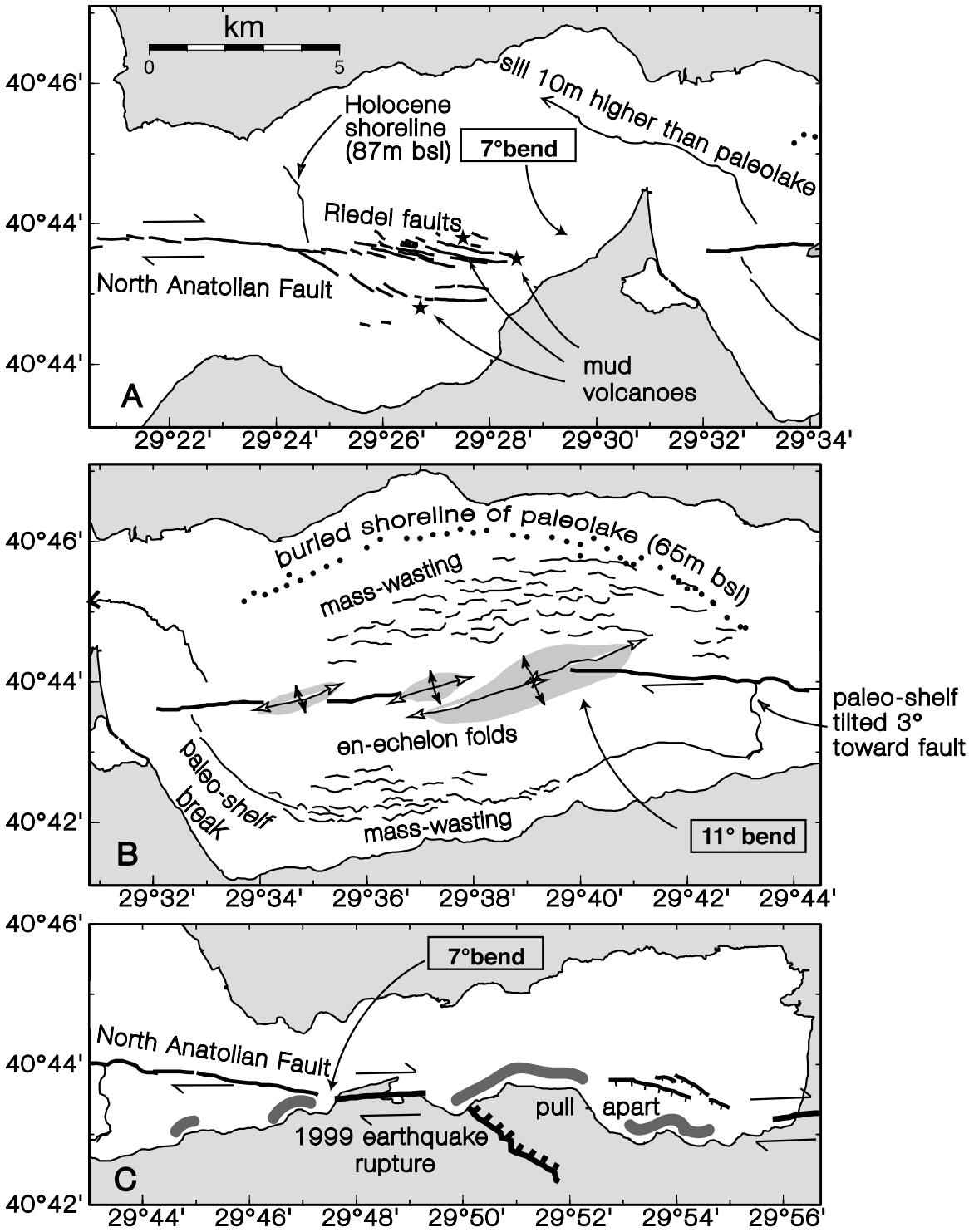

Figure 3. Geologic interpretations of the bathymetric maps in Figure 2: (a) western basin, (b) central basin, and (c) eastern basin. Thick gray lines in Figure 3c indicate shorelines that subsided or were affected by lateral spreading during the 1999 earthquake [*Emre et al.*, 2003a; *Rothaus et al.*, 2004].

1997; *Aksu et al.*, 1999; *Çagatay et al.*, 2000]. The base of these two inclines thus marks the boundary between wave cut platform and relict sea cliff, a morphological feature known as ''shoreline angle'' [*Lajoie*, 1986]. The recovery with a gravity core (located in Figure 6) of an assemblage of pebbles near the crest of that incline in Izmit Gulf does supports the interpretation of an ancient shoreline [*Polonia et al.*, 2002; *Çagatay et al.*, 2003]. The shoreline angle SW of Istanbul is located 4–5 km away from the main branch of the North Anatolian Fault [e.g., *Le Pichon et al.*, 2001] and is probably not significantly affected by fault tectonics (Figure 7). Its depth of 87 m thus is a reference for

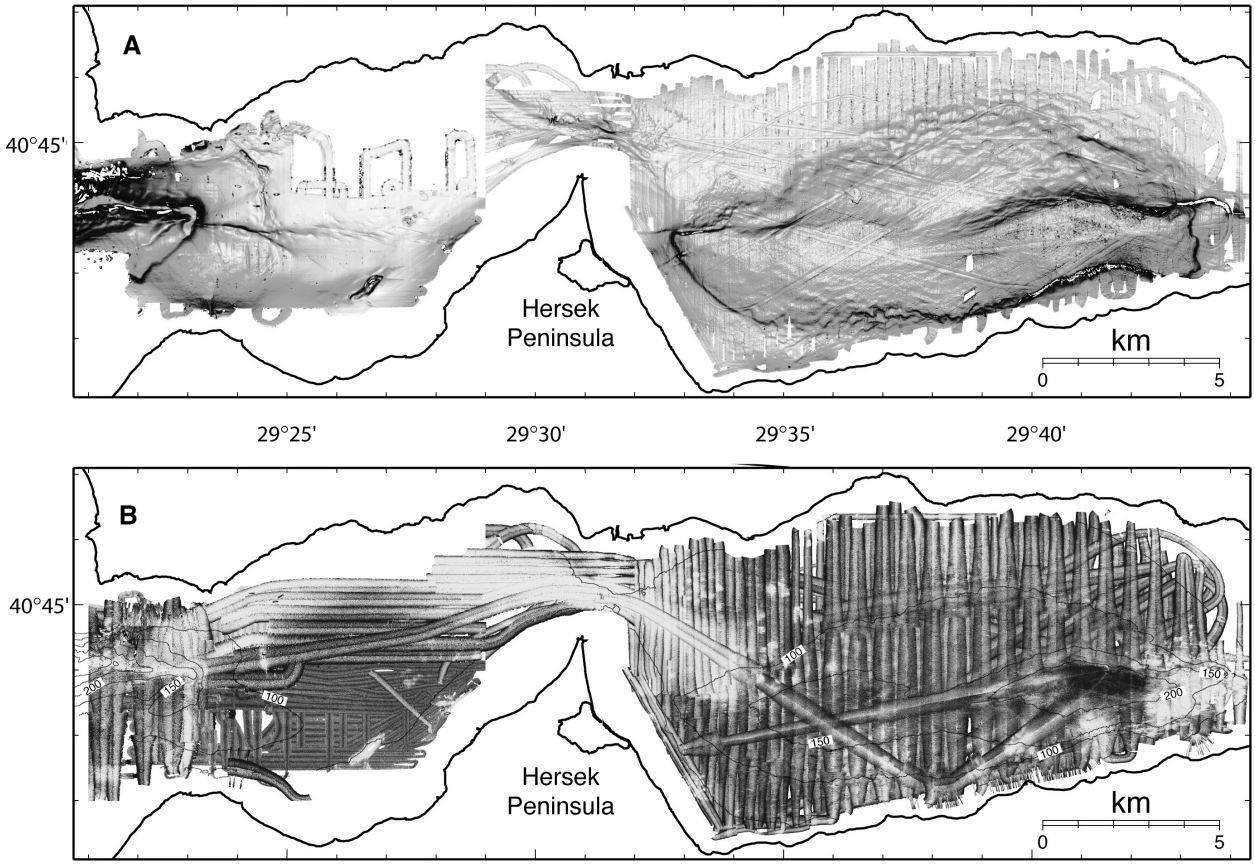

Figure 4. (a) Seafloor slopes in the western and central basins. Light shading indicates subhorizontal bottom, and darker shading indicates steeper slopes. Escarpments are highlighted as dark lineaments. (b) Acoustic backscatter for the same area. Darker shading indicates acoustically nondiffractive areas; these are typically associated with soft and/or smooth seafloor. Lighter shading indicates acoustically diffractive seafloor; this is typically associated with hard and/or rough seafloor, such as may be associated with ground ruptures. Isolated highly reflective swaths are artifacts. Evidence for disruption of the surface sediments along the main fault trace is lacking, except for the eastern end of the central basin.

the level of the Marmara paleolake during the LGM. The slightly greater depth of the paleoshoreline identified in western Izmit Gulf (Figure 6) indicates that since the LGM, the northern fault block subsided a small amount: 6–8 m subsidence within 1 km from the fault trace, and ~2–4 m subsidence a few kilometers away from the fault. Material collected just above the brackish/marine transition in three cores (including a core sited on the paleoshoreline itself) during expedition MARMARA20001 indicate tightly grouped C-14 ages of 10,100 to 10,850 ± 55 years (uncorrected). A corrected age of 11,500–12,000 years BP for the transgression of the Marmara paleoshoreline by Mediterranean waters is compatible with independent age determinations reported in *Çagatay et al.* [2000] and implies a subsidence rate of the northern fault block that is slower than 1 mm/yr. The presence of gas-charged sediments south of the fault makes it difficult to detect the same shoreline from the chirp records beneath the thick Holocene cover. Nonetheless, where gas is absent, chirp profiles indicate that the base of the Holocene drape near 29°24′E is as much as 30–40 m deeper than north of the fault (Figure 5). A very tight grid of Chirp profiles collected during expedition MARMARA2001 precisely outlines beneath the Holocene drape a paleoriver that carved its channel across the erosional surface [*Polonia et al.*, 2004]. This ancient river meandered immediately east of the paleoshoreline, and is presently offset right laterally across the main fault branch and its southern splay by 80 m and 10 m, respectively [*Polonia et al.*, 2004]. However, except for these two discrete offsets, its course does not appear to have been affected by the fault geometry, suggesting that the erosional surface was roughly planar across the fault zone during the LGM. The preservation of that channel on both sides of the fault also implies that the paleoshoreline south of the fault lies west of it. Assuming that the marine transgression of the LGM surface occurred around 11.5–12 kyr, the difference in elevation of 30–40 m across the fault trace implies that the southern fault block subsides at an average rate of 2.5–3.5 mm/yr near the paleoshoreline. In contrast, the base of the Holocene is not significantly offset across the fault near 29°27′E, 3 km further east.

3.1.4. Mud Volcanism

[12] Closer to Hersek peninsula, three large mounds straddle the fault segments and protrude from the smooth sedimented surface (Figures 8 and 9). These three mounds display high acoustic reflectivity, an indicator of rough

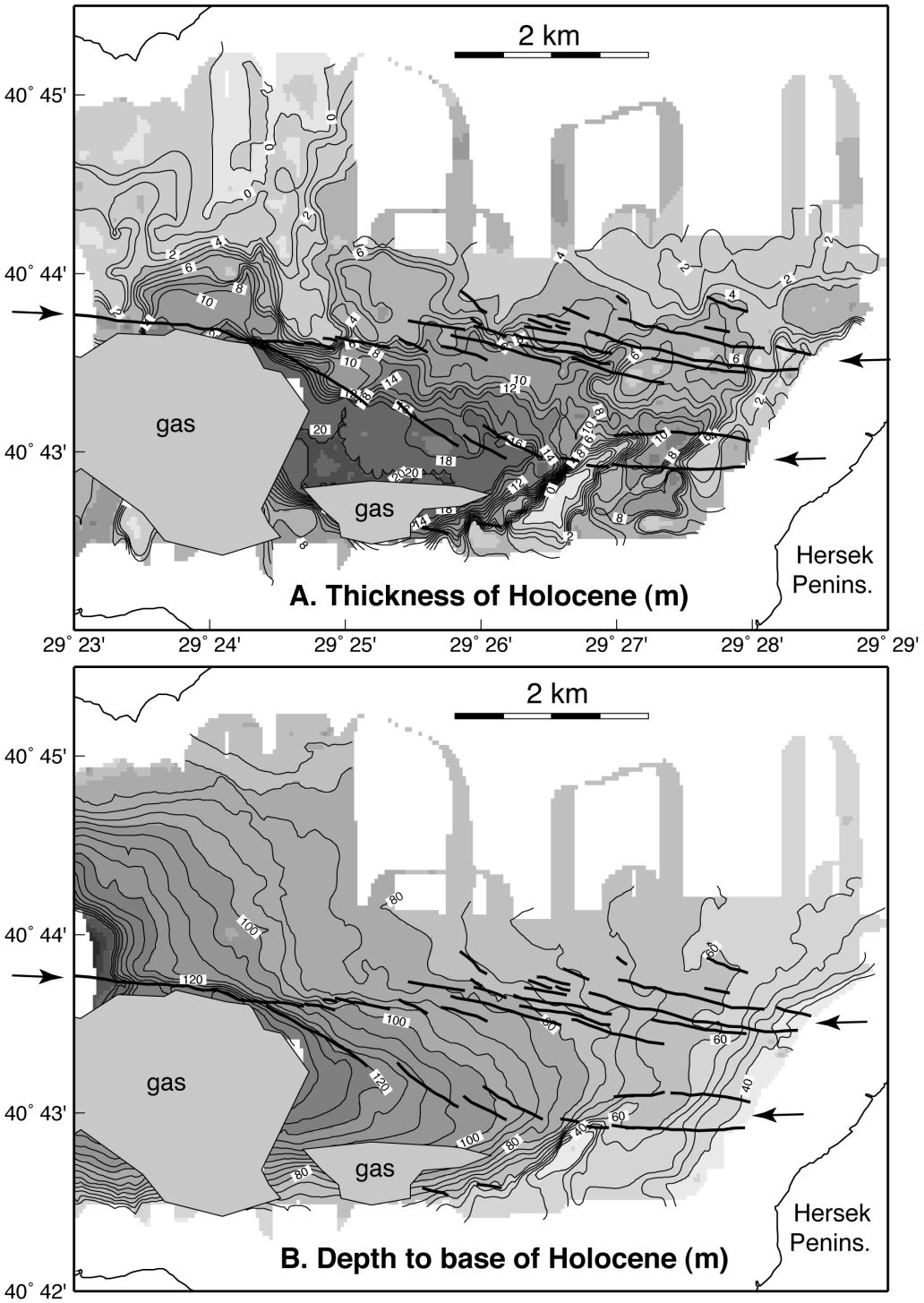

Figure 5. (a) Thickness of the Holocene drape in the western basin derived from the grid of chirp profiles collected during expedition MARMARA2000 (mean track spacing 150 m). Arrows point to the main branch of the North Anatolian Fault and a splay. Contour interval is 2 m. Gray patches correspond to areas where bottom penetration is obscured by the high gas content of the sediments. Sound velocity through the Holocene drape is assumed to be the same as water (1500 km/s); errors introduced with this assumption are less than 5%. Note the asymmetry in the thickness of the drape across the fault. (b) Topography at the base of the Holocene drape, obtained by subtracting the grid in Figure 5a from the bathymetric grid. Contour interval is 5 m. Vertical deformation across the main branch increases westward.

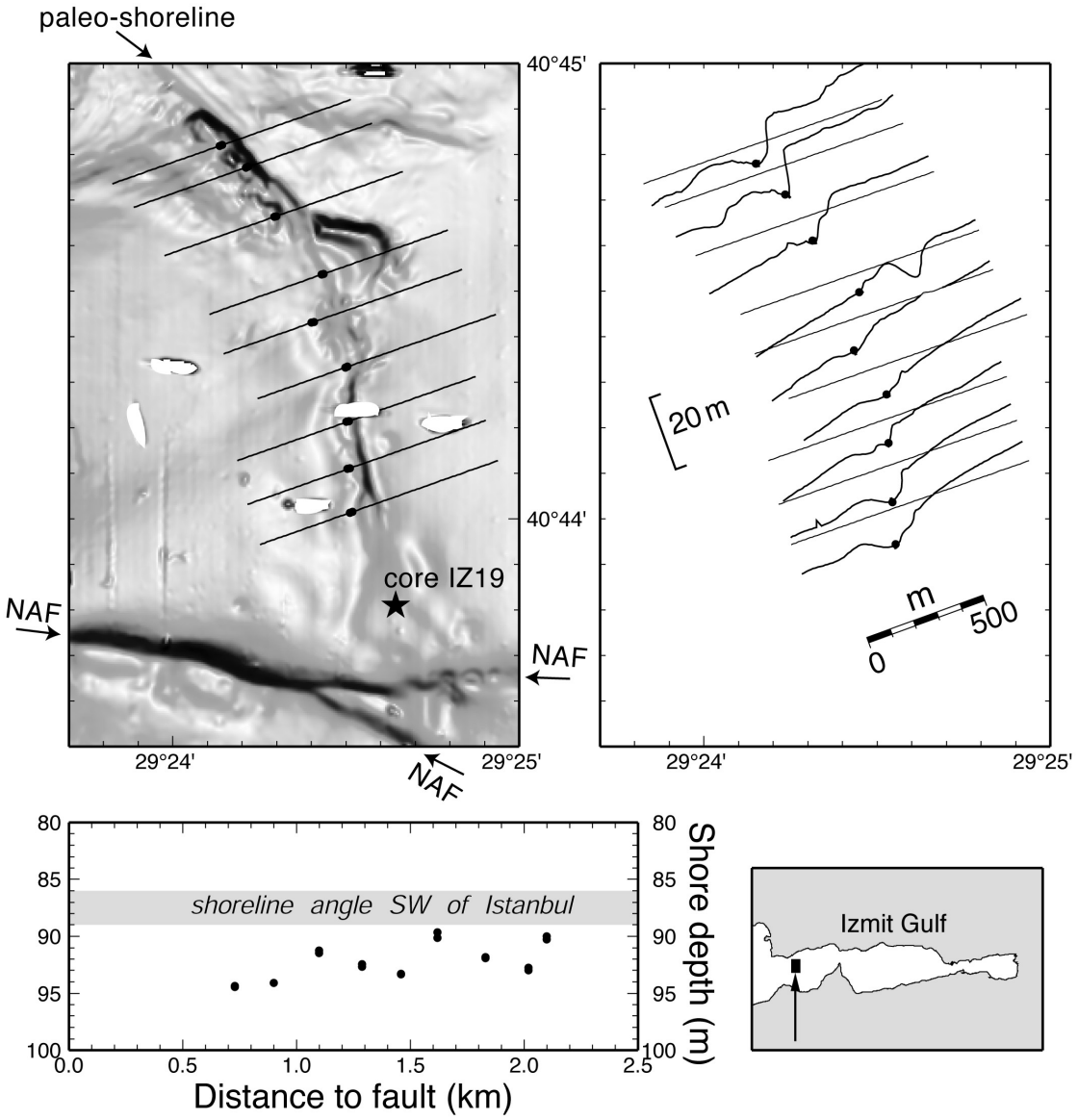

Figure 6. Paleoshoreline mapped in the western basin. (top left) Seafloor gradient, with darker shading indicating steeper slope. The escarpment striking NNW corresponds to the same paleoshoreline as in Figure 7. Lines indicate the location of the bathymetric profiles displayed at right. Dots indicate picks for the shoreline angle, and arrows point to the North Anatolian Fault (NAF). The short, arcuate depression east of the shoreline is a river channel that has been truncated by the lake shore; the star locates gravity core IZ19 that sampled a pebble assemblage characteristic of a shoreline [*Polonia et al.*, 2004]. (top right) Bathymetric profiles taken perpendicular to the submerged shoreline (located at left). Dots indicate the shoreline angle picks. Vertical exaggeration is 15. (bottom left) Depth of shoreline angle versus distance to the North Anatolian Fault. (bottom right) Index map; arrow points to the area displayed above.

seafloor and/or coarse surficial material. The northern mound is composed of several cones across an area 0.5 km wide (Figure 9a). It is less than 5 m high and is surrounded by a shallow, 1-m-deep moat. A grab sample taken from the top of the largest of the cones during expedition MARMARA2000 recovered oyster shells, various benthic fauna, and unconsolidated mud. The morphology of that mound is typical of mud volcanoes. The southern mound is the largest and is elongated in a NE-SW direction (Figure 9c). It is 1.2 km long, 0.3 km wide, and 40 m high. Inspection with a towed camera across its 24-m-deep summit revealed scattered oyster shells sticking out of the mud cover. Only the western edge of the third mound could be mapped, as it is located only 1 km from shore (Figure 9b). Nonetheless, on the basis of the extent of the mapped area, we infer that it may have similar dimensions to the southern mound. It is located on the main fault branch and rises a minimum of 10–15 m above the surrounding seafloor.

[13] Mud volcanoes are constructs produced by the ascent of gas-rich and/or fluid-rich overpressured fine-grained sediments, and occur in association with faults, folds, or

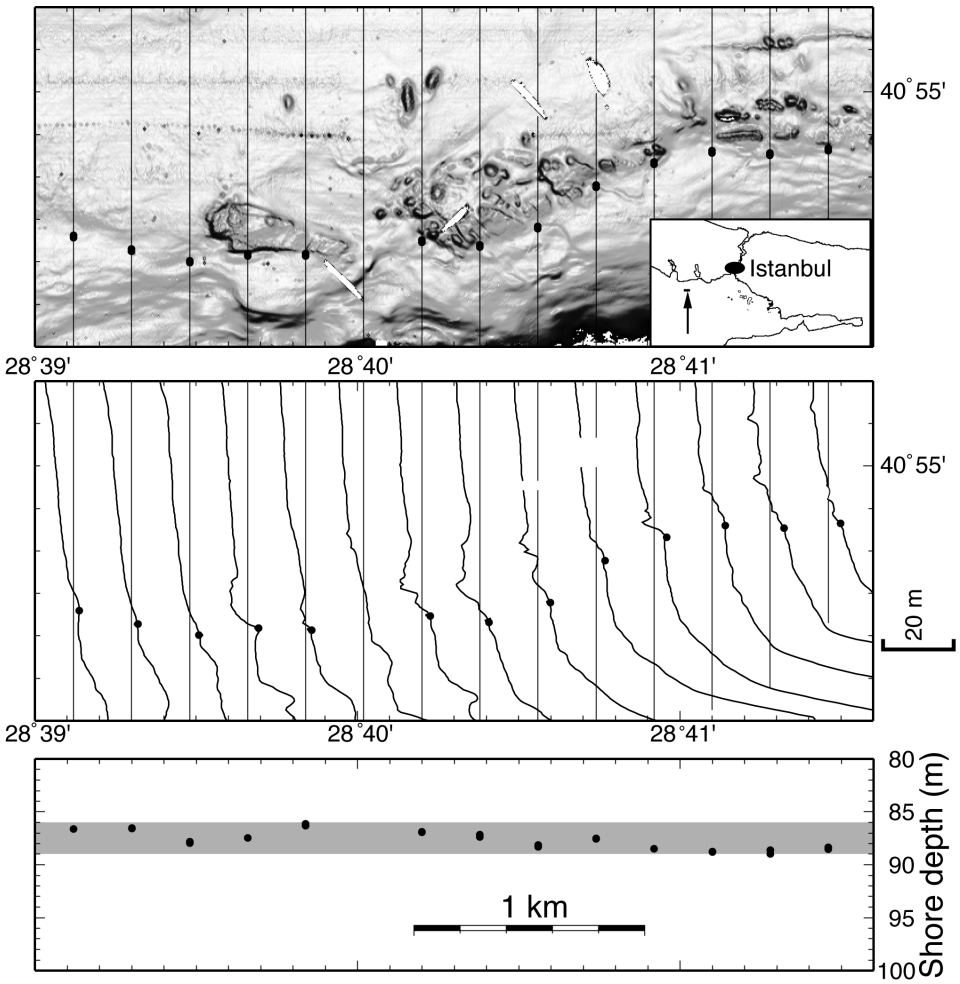

Figure 7. Paleoshorelines mapped southwest of Istanbul. (top) Seafloor gradient, with darker shading indicating steeper slope. Area is located in inset at bottom right (arrow). NS lines locate the bathymetric profiles displayed below. Dots indicate the shoreline angles picked from these profiles. These picks delimit a smooth seafloor to the south from rough seafloor to the north. Rougher texture is interpreted as outcropping bedrocks that may have been attacked by wave action along the shore of Marmara Lake during the Last Glacial Maximum. (middle) Series of NS depth profiles extracted from the bathymetry. Each profile is located directly beneath its corresponding map view location from the top map, with "up" to the left. Vertical exaggeration is 12. Ticks indicate picks for the shoreline angle. (bottom) Depth of shoreline angle versus longitude.

subsurface mud diapirs [*Dimitrov*, 2002; *Kopf*, 2003; *Somoza et al.*, 2003; *Hughen et al.*, 2004]. In itself, the morphology of the southern and eastern mounds is not diagnostic of mud volcanoes and could simply indicate folding of the surface strata along the right-lateral North Anatolian Fault, as proposed in [*Polonia et al.*, 2004]. However, a combination of factors suggests that these are mud volcanoes. First, their heights (20–40 m), lengths (~1 km), steep flanks (>15°), and high-amplitude acoustic backscatter are common features of mud volcanoes [e.g., *Dimitrov*, 2002; *Somoza et al.*, 2003]. Second, chirp profiles do not show evidence for folded strata beneath them, although the surrounding layers are upturned in their vicinity (Figure 10). Instead, internal reflectors are lacking or chaotic, as is typical of mud volcanoes. The absence of a Holocene drape across the mounds (Figures 5a and 10) is also compatible with recurring expulsion of subsurface sediments. The presence of overpressured sediments in this area is suggested from the widespread liquefaction across Hersek peninsula reported during the 10 July 1894 earthquake [*Ambraseys*, 2001]. Finally, the three mounds are elongated to the NE, parallel to the least compressive stress for this section of the right-lateral North Anatolian Fault. Diapiric ridges and mud volcano fields are common on accretionary prisms and broad shear zones and are similarly elongated parallel to the least compressive stress [*Griboulard et al.*, 1991; *Somoza et al.*, 2003; *Hughen et al.*, 2004].

[14] Careful sediment sampling and geochemical analysis should confirm whether these features are mud volcanoes. If indeed they are, they should be associated with folded and/or diapiric structures in the deeper subsurface, in agreement with the slightly compressional regime we infer near this 7° bend of the North Anatolian Fault (see section 6). Possibly, these mud volcanoes become activated when large earth-

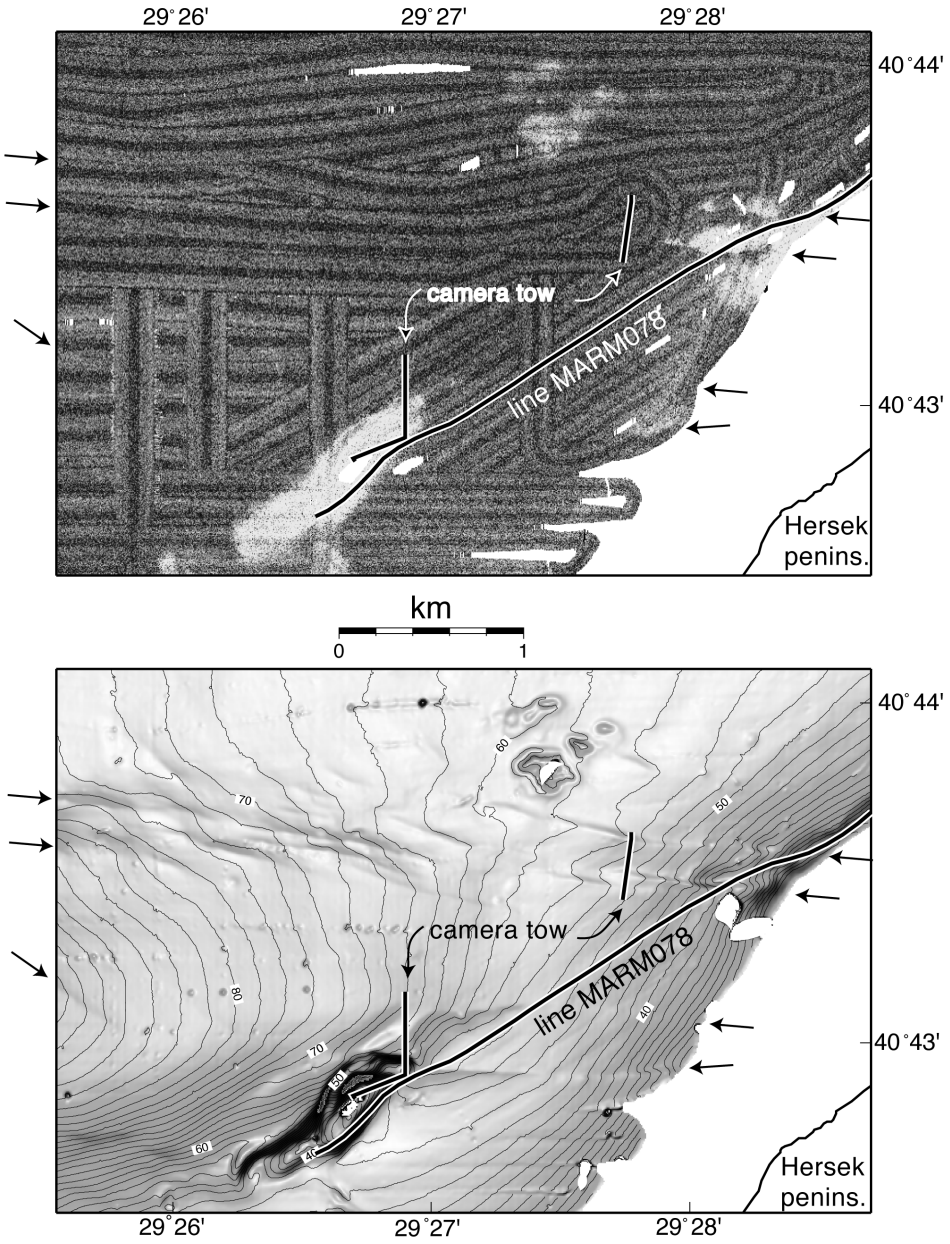

Figure 8. Detailed multibeam data for the area west of Hersek peninsula. Arrows point to en echelon segments of the North Anatolian Fault. Tracks from a camera tow are indicated with the black-on-white lines. Chirp line MARM078 is displayed in Figure 10. (bottom) Seafloor gradient overlaid with 2 m contour intervals. Lineaments with steeper slopes (darker shades) outline the various fault segments. (top) Corresponding acoustic backscatter data. Lighter shading indicates high acoustic backscatter. The data do not outline any of the fault segments, as would have been expected if they ruptured recently. High-backscatter values, on the other hand, are associated with three mounds that straddle the fault segments.

quakes rupture the North Anatolian Fault. Accordingly, gas release has been documented in association with seismic events for various offshore locations around the world [*Clifton et al.*, 1971; *Field and Jennings*, 1987; *Hasiotis et al.*, 1996; *Kopf*, 2002; *Chapron et al.*, 2004; *Hieke*, 2004].

3.2. Central Basin

3.2.1. Fault Geometry

[15] An escarpment up to 90 m high bounds the northern side of the 210-m-deep central (Karamürsel) basin (Figures 2b and 11). It is aligned with the main fault trace in western basin and most likely corresponds to the same branch. It strikes N086°E in the western half of the basin and bends to a N097°E orientation in the eastern half (Figure 3b). At the east and west ends of the basin, the fault trace is sharply defined by a south facing scarp, and locally, by a narrow groove in that scarp. In the central portion of the basin, the escarpment is overprinted by three ~500-m-wide and ~10-m-high gentle ridges (Figure 11). These right stepping ridges are oriented 10°–15° clockwise to the main

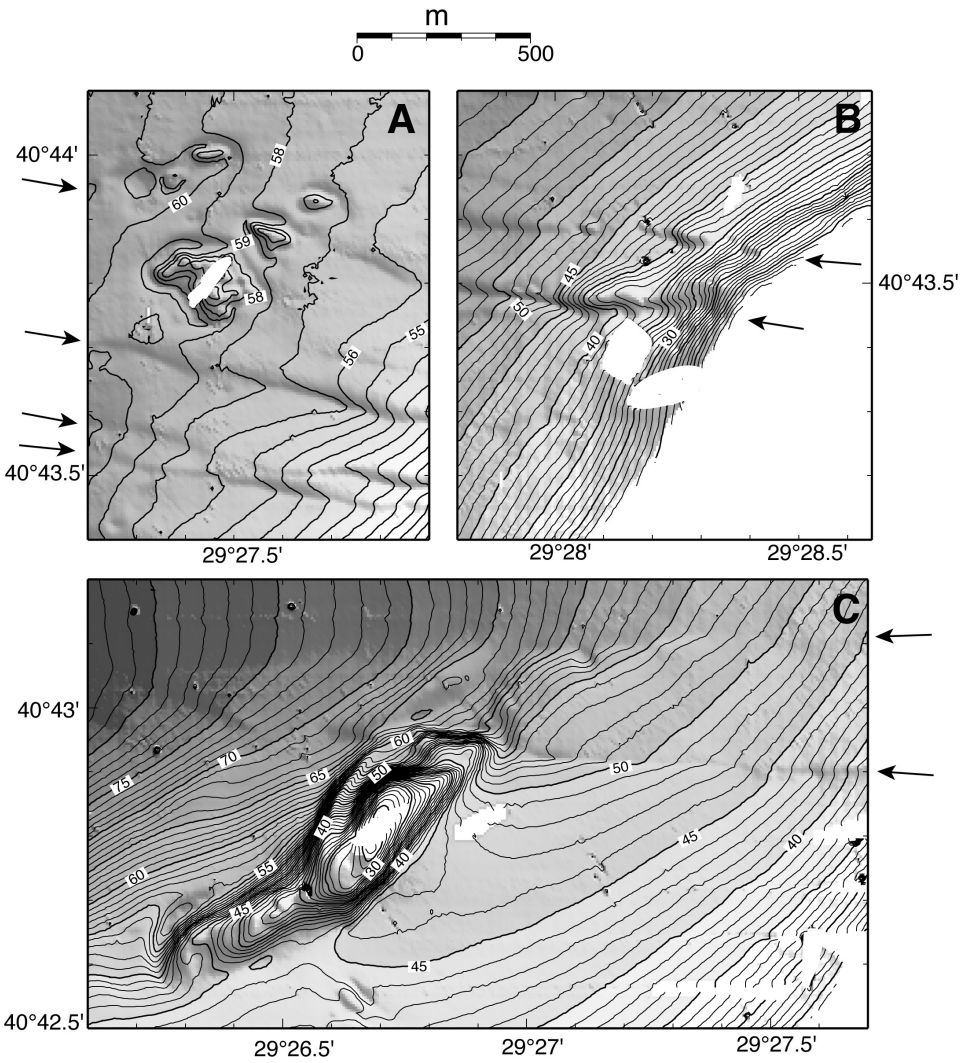

Figure 9. Detailed bathymetry of three mounds west of Hersek peninsula: (a) northern mound, (b) eastern mound (only its steep edge could be mapped), and (c) southern mound. Contour interval is 1 m. Arrows point to short en echelon segments of the North Anatolian Fault. Mounds are elongated to the NE, in the direction of the least compressive stress for a right-lateral transform.

fault trend, compatible with the orientation of folds expected to develop across right-lateral transform faults [*Sylvester*, 1988; *Tchalenko*, 1970]. The largest fold forms a restricting sill between the west and east halves of the basin.

[16] The south facing escarpment progressively decreases in height toward the coastlines of Hersek peninsula to the west, and Gölcük to the east. It meets the Gölcük shoreline where the 17 August 1999 earthquake land rupture reached 4.5–5 m of right-lateral slip, some of the largest recorded along the emerged portion of the fault (Figure 2c). A series of NS transects across central basin shows that maximum depths occur systematically at the base of the fault scarp (Figure 11). Available seismic profiles indicate a progressive tilting of the basin infill toward that fault scarp (Figure 12, line I-44). Both observations suggest that the North Anatolian Fault accommodates significant amount of dip slip (down to the south) through central basin.

3.2.2. Marginal Mass Wasting

[17] The periphery of the basin displays a lumpy, scalloped bathymetry (Figures 2b, 4, and 11). The corresponding subsurface structures consist of strata that are deformed into a series of convex upward hummocks and intervening steep-sided depressions, draped by Holocene deposits (Figure 12, line I-33). This may be indicative of subsurface faulting, in agreement with models invoking numerous closely spaced faults on the basis of high-resolution seismic surveys [*Gökasan et al.*, 2001; *Alpar and Yaltirak*, 2002; *Kusçu et al.*, 2002]. However, the multibeam bathymetry indicates that most hummocks extend laterally less than 1–2 km, suggesting that they are surficial features. Similar hummocky features imaged in high-resolution seismic records in various tectonically quiet areas around the world have been interpreted as seabed pockmarks formed by gas escaping from the sediments [*Kelley et al.*, 1994; *Çifçi et al.*, 2003], or as fluidization pipes cutting through rapidly deposited sediments [*Davies*, 2003]. Gas-charged sediments in Izmit Gulf are evident in the chirp records (Figure 12) [*Kusçu et al.*, 2002], and must favor widespread fluidization and/or gas release during large earthquakes of the North Anatolian Fault. Accordingly, *Ambraseys* [2001, p. 119] reports that during

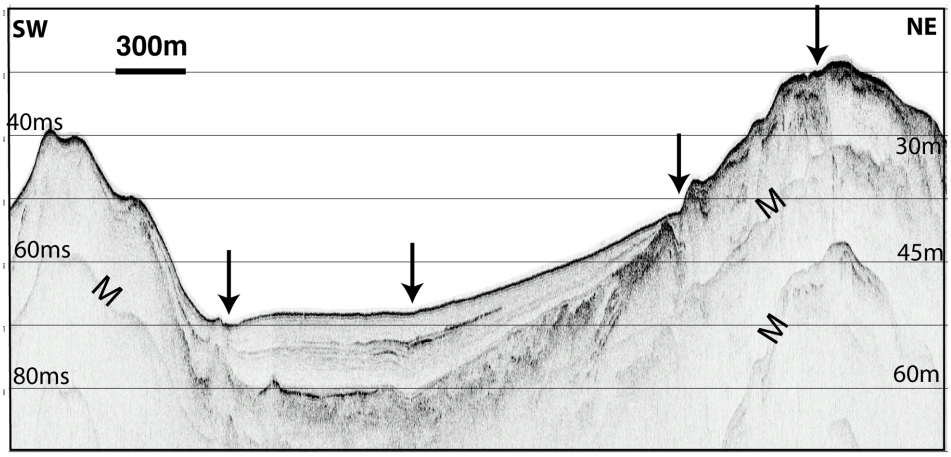

Figure 10. High-resolution seismic (chirp) profile MARM078 across two large mounds west of Hersek peninsula. Profile location is given in Figure 8. Vertical exaggeration at the seafloor is 34. Arrows indicate crossings of en echelon segments of the North Anatolian Fault. "M" indicates multiples; the towed chirp profiler recorded both sea surface and seafloor multiples. Note the lack of coherent horizons beneath the mounds and the lack of a Holocene drape over them.

the large 10 July 1894 earthquake, "at Hersek, most farmhouses were destroyed and the ground liquefied." The 17 August 1999 Izmit earthquake also induced ground liquefaction and lateral spreading along the southeastern shore of central basin [*Lettis et al.*, 2002; *Emre et al.*, 2003a; *Rothaus et al.*, 2004] and several gas plumes were detected in the water column from seismic profiling [*Alpar*, 1999]. Hence the lumpy texture around the basin periphery may preferentially reflect mass wasting and fluidization of gas-charged sediments, probably induced by earthquake events. This scenario does not preclude that some of the sedimentary structures are rooted on subsidiary faults.

3.2.3. Submerged Shoreline

[18] Most of the chirp profiles across the northern shelf indicate the presence, beneath the Holocene cover, of a sediment lens a few meters thick and a few hundred meters wide (Figure 12, lines I-15 and I-33). The top of that lens is subhorizontal and its north edge maintains a constant depth of 64 m ± 2 m (Figure 13), suggesting that its deposition was controlled by water level. This constant depth also implies that the lens has not been offset or tilted since its deposition. This feature may represent prograding beds that formed just below wave base when water level in central basin was slightly higher than 64 m [*Çagatay et al.*, 2003]. The strait north of Hersek peninsula is crossed by a channel that describes a broad meander down into the western basin (Figures 2a and 13). Chirp profiles show that this channel is carving the same erosional surface that underlies the sediment lens (Figure 14). Channel and lens may therefore have been contemporaneous features. A possible scenario is that when the level of the Marmara Sea was deeper than 64 m, a lake occupied the central basin that drained into the western basin via the channel, favoring the deposition of the sediment lens beneath wave base. An alternate scenario is that this paleoshoreline formed during a world sea level stillstand at around 60 m, as proposed by *Çagatay et al.* [2003]. Regardless, both models carry identical implications with regards to the uplift of the Hersek peninsula. The sill depth north of the peninsula is presently 54 m (Figure 13), 10 m shallower than the upper level of the sediment lens. Thus, while the horizontality of the sediment lens east of 29°33′E indicates that it has not deformed since its deposition, the area north of Hersek peninsula may have uplifted by up to 10 m. The world's sea level reached ∼64 m at around 10 kyr BP [*Fairbanks*, 1989], implying a mean uplift rate of ∼1 mm/yr for the sill. Alternatively, the sill may be partially filled by a recent landslide (Figures 13 and 14), in which case the uplift rate north of the fault could be much lower, or even null.

3.2.4. Ancient Shelf Break

[19] The southern side of the central basin is defined by a continuous escarpment that roughly parallels the shore, except between 29°35′–39′E where mass wasting disrupts its continuity (Figures 2b and 4). To the west, the escarpment curves northward and terminates against the main EW fault branch. To the east, the escarpment bends sharply northward and also abuts the EW branch at 29°43.2′E. The escarpment is everywhere 15–90 m high and steeper than 10°. Because of this steepness, shallow-penetrating chirp profiles did not provide useful images of subsurface geological structures. The crest of the escarpment approximately matches the 72 m depth contour in the western section of the basin, but its height and slope are atypical of submerged shorelines. Its sinuous plan view geometry is also difficult to reconcile with that of a fault scarp, although it may be locally fault controlled. Instead, we interpret that escarpment as marking a shallow shelf break that developed when the central basin was occupied by a lake with a water level around 64 m, as discussed above. This interpretation is partly supported by the presence of shelf breaks with similarly sharp outlines along narrow continental shelves [*Slater et al.*, 2002; *Gardner et al.*, 2003] and lakes [*Gardner et al.*, 2000; *Morgan et al.*, 2003]. The lack of a well-defined shelf break north of the fault may result from its destruction by gravitational sediment failure and sediment fluidization. Provided this paleoshelf break was nearly horizontal at the time of its formation, present depth variations along its length provide

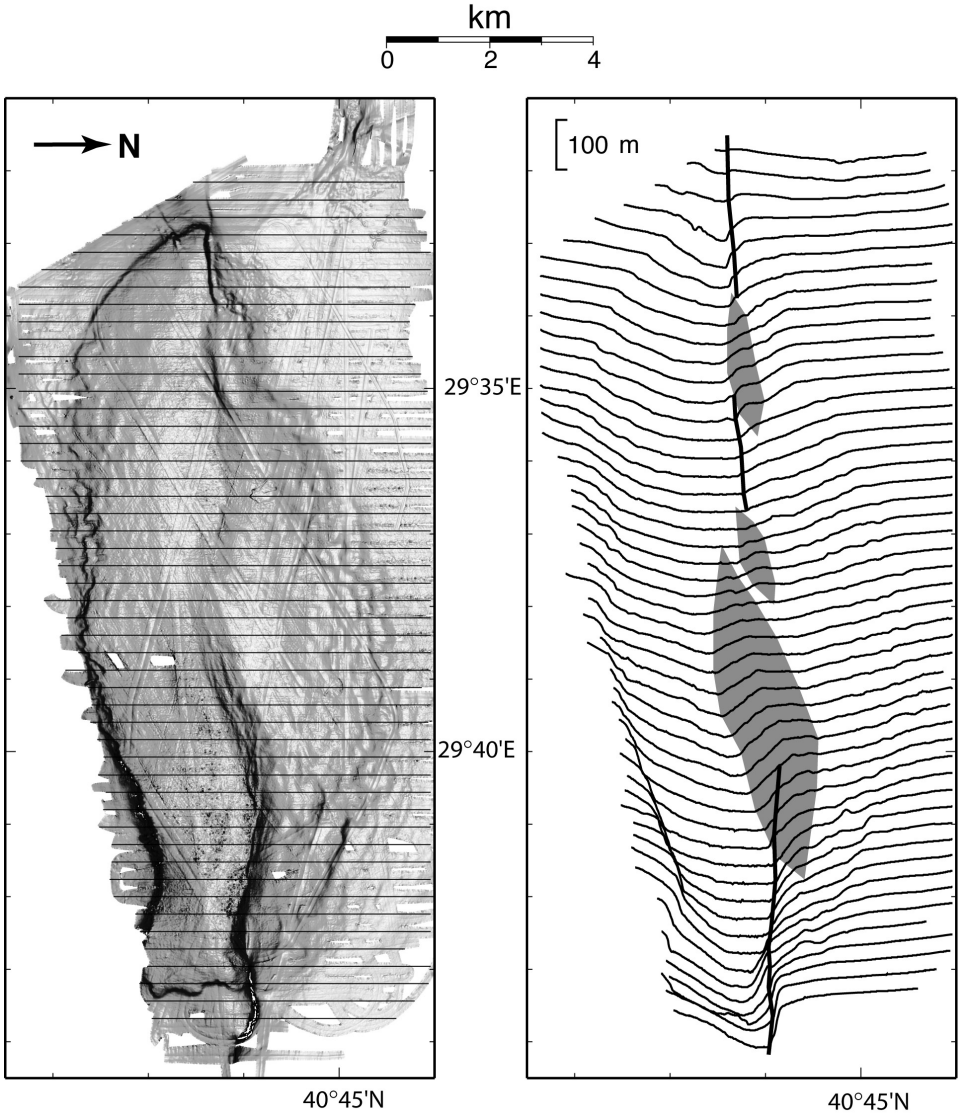

Figure 11. Series of depth sections highlighting the fine-scale physiography of the central basin. (left) Slope gradient (darker shading indicates steeper slopes). Lines locate the bathymetric profiles displayed at right. North is to the right. (right) Depth profiles shown with a vertical exaggeration of 10 in their approximate geographical position. The thick line locates the master branch of the north Anatolian Fault, and the shaded areas outline three en echelon right stepping folds. The arcuate escarpment to the south (left) is interpreted as an older shelf break (section 3.2); it is disrupted by mass wasting in the middle section.

some clues with regards to vertical tectonics. Chirp profiles indicate that the Holocene cover at the shelf break is 5–10 m thick, so depth variations in excess of 10 m should imply vertical motion. From 29°40′E to 29°42′E, the shelf break deepens by about 10 m. It turns northward at 29°43.2′E and deepens steadily by 80 m toward the fault scarp (Figure 15). This 3° northward dip is consistent with other indicators (discussed above) of tectonic subsidence of the southern fault block. Rapid flooding of the 60–65 m paleolake by marine waters must have occurred around 10,000 years ago [*Fairbanks*, 1989], at which time the paleoshelf break would have become inactive. Therefore the 80 m deepening of the paleoshelf break toward the fault plane implies a subsidence rate of ~8 mm/yr. The lack of any significant depth variation along the remaining of the paleoshelf break suggests, however, that rapid subsidence is localized.

3.3. Eastern Basin

[20] The eastern (Golcuk) basin is only 40 m deep and 6 km long (Figure 2c). The surface rupture from the 17 August 1999 continues beneath the basin near its southern shore with a N80°–90°E orientation and a right-lateral displacement of 3.0–3.2 m [*Barka et al.*, 2002; *Emre et al.*, 2003a] (Figures 2c and 3c). Another on-land rupture occurred 3 km west of the basin and produced a 3.5-km-long northeast facing scarp with normal and right-lateral displacement (1.5–2 m and 0.5–1.5 m, respectively.) Coseismic NE tilting and hang-

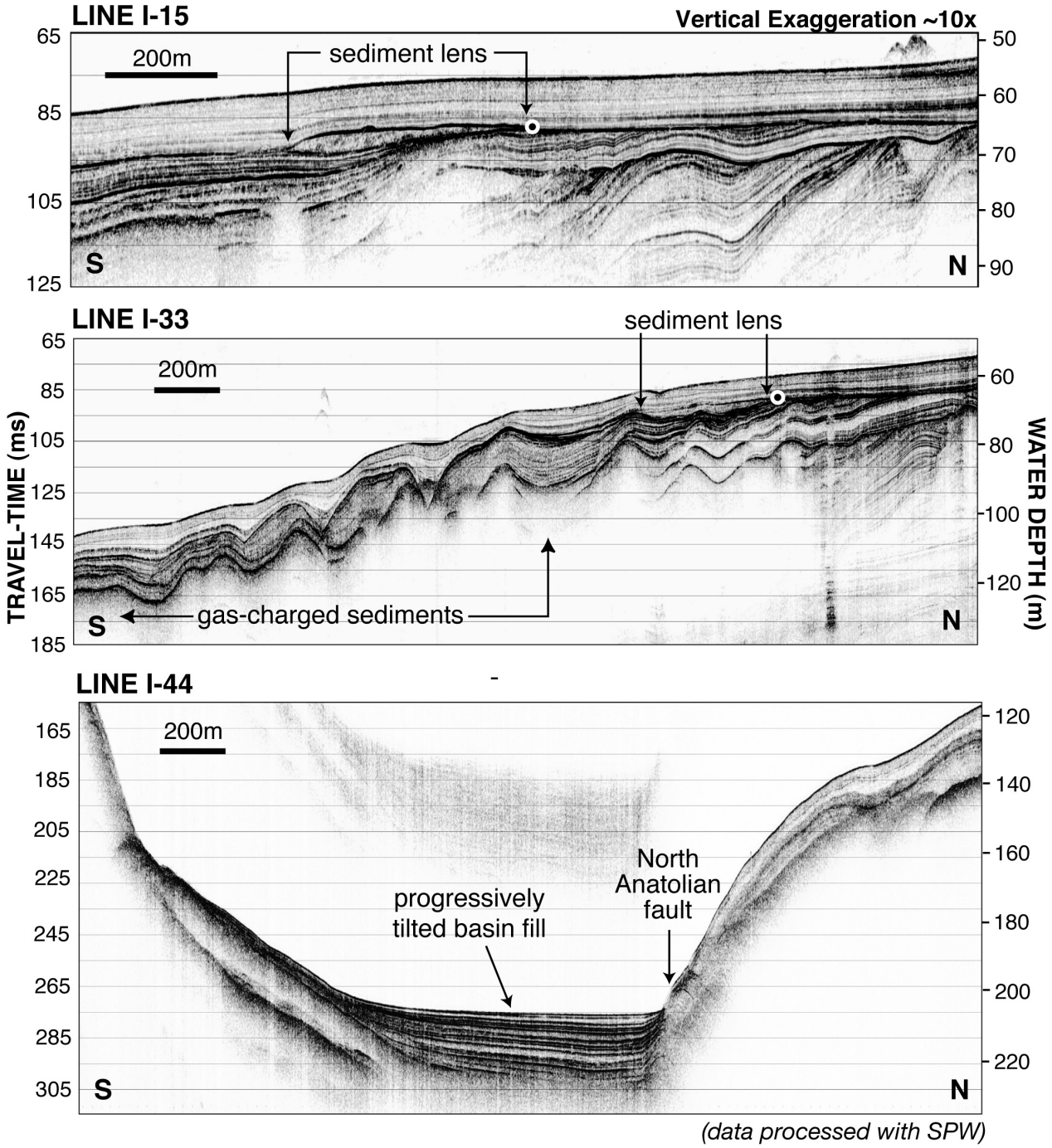

Figure 12. Sample chirp profiles across the central basin, located in Figure 13. The sediment lens beneath the Holocene drape at 85 ms (64 m) on lines I-15 and I-33 is present on most profiles. White circles mark the northern edge of that lens (also located in Figure 13). The strong seismic reflector obscuring deeper returns in the southern half of line I-33 is interpreted as marking the top of gas-charged sediments; the convex upward hummocks in the strata above the gas-charged interval are interpreted as resulting from sediment fluidization. Line I-44 images the flat bottom of the central basin; note how beds become progressively tilted toward the North Anatolian Fault.

ing wall subsidence along its length resulted in the drowning of the shoreline along the SW corner of the basin (Figure 3c) [*Barka et al.*, 2002]. Multibeam bathymetry reveals the presence midway between these land ruptures of two 2–5 m high, south facing escarpments striking NW-SE (Figure 2c).

[21] A single transect with a towed camera across the largest scarp did not detect any fresh rupture and revealed instead a gently sloping seafloor draped with mud [*Polonia et al.*, 2002]. A lack of earthquake rupture along that escarpment would be surprising considering that prominent ruptures occurred on either side of the basin. Possibly, the

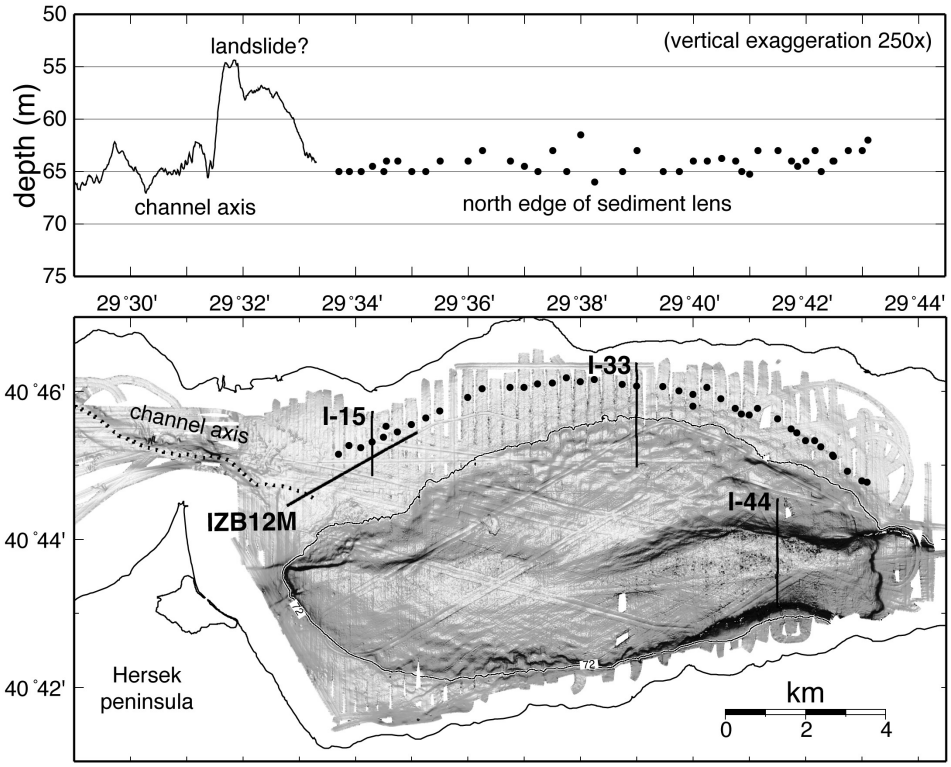

Figure 13. Some markers of vertical deformation in the central basin. (top) Depth of the northern edge of the sediment lens versus longitude (dots). The solid line indicates the depth of the channel axis. Vertical exaggeration is 250. The deposition of the horizontal sediment lens was probably controlled by a water level in the central basin that was just slightly shallower than ~64 m depth (see text). The sill north of Hersek peninsula is ~10 m shallower than the lens; it may have uplifted by that much since it was carved down; alternatively, it may be partially filled in by a landslide (see Figure 14). (bottom) Seafloor gradient in the central basin (darker shading indicates steeper slopes). The three chirp profiles displayed in Figure 12 are labeled. Dots indicate the northern extent of the shallow sediment lens picked from the chirp profiles. The arcuate escarpment delimiting the basin to the south approximately matches the 72 m depth contour in the western half of the basin and progressively deepens eastward. North of the fault, the 72 m contour traverses the zone of hummocky seafloor. Dotted line indicates the axis of a channel that connects the eastern and western basins.

1999 rupture is discontinuous and was missed by the transect. Indeed, the towed camera imaged fresh-looking polygonal cracks on the flat basin floor at the base of the scarp that may be diagnostic of sudden fluid or gas release during the 1999 earthquake. Accordingly, sediments in that basin are strongly gas charged and several gas plumes were detected in the water column from high-resolution seismic profiles acquired in March 2000 [*Kusçu et al.*, 2002].

[22] The patterns described by the land ruptures and the submarine scarps are that of a pull-apart system, with dip-slip motion partitioned between two antithetic, NW striking faults (Figure 3c). This pull-apart geometry corresponds to a 1.2 km releasing right step over of the North Anatolian Fault. It contrasts with the fault geometry in Central and Western basins, where dip slip is accommodated in the plane of the transform fault.

4. Fault Trace Across Hersek Peninsula

[23] The 17 August 1999 earthquake produced minor offsets and cracking (<5 cm) across Hersek peninsula that have been interpreted as sympathetic slip rather than surface rupture [*Witter et al.*, 2000; *Lettis et al.*, 2002]. Paleoseismic trenches excavated on the peninsula near latitude 40°43.3′N did not provide conclusive evidence for Holocene faults, and the precise location of the northern branch of the North Anatolian Fault across Hersek remained somewhat controversial. Simple extrapolations of the submarine branches imply, however, that the main fault describes a ~7° bend across Hersek peninsula around latitude 40°43.5′N, near the northern limit of the Hersek lagoon (Figures 2a and 3a). No significant step over is required to match these eastern and western submarine fault traces. The southern fault splay mapped west of the peninsula intersects the shoreline near latitude 40°43′N and may merge with the main branch somewhere on the peninsula; possibly, it corresponds to the WNW "Yalova fault segment" proposed on the basis of geomorphic lineaments [*Witter et al.*, 2000; *Lettis et al.*, 2002]. The existence of multiple splays could explain the difficulties encountered in locating significant fault branches with paleoseismic trenching. Evidence of earlier fault rupture may also be obscured by soil liquefaction, such as that produced across Hersek peninsula in the 10 July 1894 earthquake [*Ambraseys*, 2001].

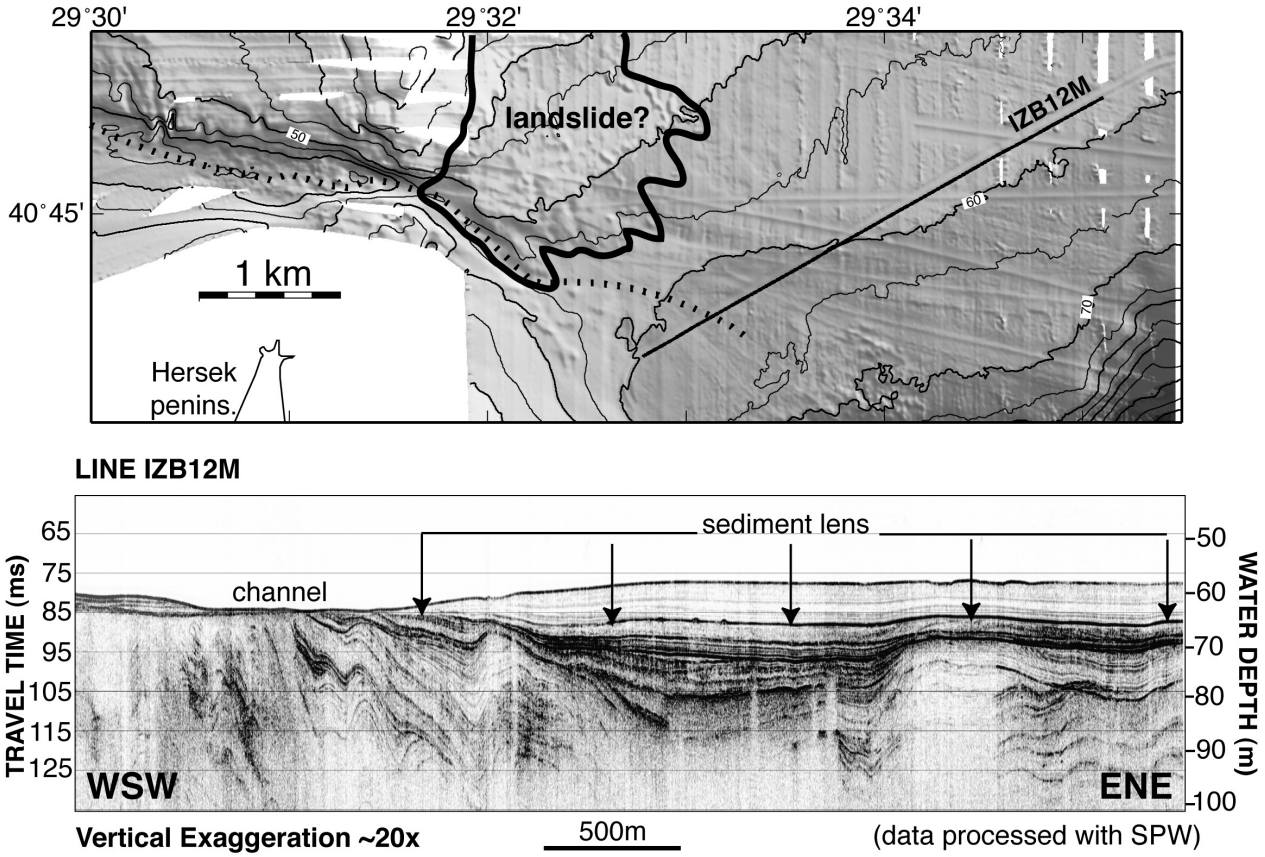

Figure 14. Details of the sill connecting the western and central basins. (top) Shaded bathymetry overlaid with 5 m contours. The dotted line indicates the axis of a paleochannel. The solid line locates the chirp profile displayed at bottom. The thick contour approximately outlines a possible landslide, as inferred from the hummocky seafloor texture visible in both the chirp and bathymetric data. NS or EW features are mostly ship track artifacts. (bottom) Chirp profile IZB12M intersecting the sediment lens in its long-axis direction (see Figures 12 and 13). The lens lies entirely beneath the Holocene drape and pinches on the channel connecting the western and central basins.

[24] Several lines of evidence suggest Hersek peninsula is uplifting, possibly as a consequence of the 7° bend. Three Quaternary marine terraces 6–8 m above sea level have been mapped across the fault zone at the northern tip of the peninsula [*Alpar and Güneysu*, 1999; *Lettis et al.*, 2002]. Although their elevations may be compatible with that of a sea level highstand during the last interglacial [e.g., *Stirling et al.*, 1998] and do not necessarily imply tectonic uplift, they are also compatible with a possible 5–10 m uplift of Hersek strait during the Holocene (see previous section). The sliver of crust bounded by the main fault and the southern splay is predicted to be under slight transpression, also implying uplift for the area. Recent fieldwork on Hersek peninsula indeed documented the presence of a series of en echelon thrust faults, interpreted to be absorbing that transpression [*Emre et al.*, 2003b]. Finally, the presence of mud volcanoes west of Hersek also indicates that the western shore is under slight transpression.

5. Western Termination of the 17 August 1999 Seafloor Rupture

[25] Significant fault slip during an earthquake will alter the static stress on adjacent fault segments and may bring them closer to rupture [*Stein et al.*, 1994]. Hence a precise knowledge of the length of fault that ruptured in a large earthquake is critical for making a reliable assessment of the seismic hazards associated with the entire fault system. Maps of active faults and records of large earthquakes are commonly used to model static stress loading across seismically sensitive areas and evaluate which fault segments may be critically stressed. Several models have been produced for the North Anatolian Fault that take into account historical and recent earthquakes [*Stein et al.*, 1996, 1997; *Nalbant et al.*, 1998; *Hubert-Ferrari et al.*, 2000; *Parsons et al.*, 2000; *Papadimitriou et al.*, 2001; *Pinar et al.*, 2001; *Parsons*, 2004]. While recent models acknowledge that the 17 August 1999 earthquake critically stressed the North Anatolian Fault beneath the Marmara Sea, the extent of the rupture beneath Izmit Gulf remains a matter of debate. The westernmost surface displacement documented on land occurs at Golcuk, at the eastern side of Central basin, where right-lateral slip reached 4.5–5.0 m [*Barka et al.*, 2002; *Lettis et al.*, 2002; *Emre et al.*, 2003a]. Despite the lack of surface rupture on Hersek peninsula, many consider that the peninsula represents a short gap and that the fault ruptured as far west as Çinarcik basin. The fact that aftershocks extended 35 km west of Hersek peninsula along a narrowly

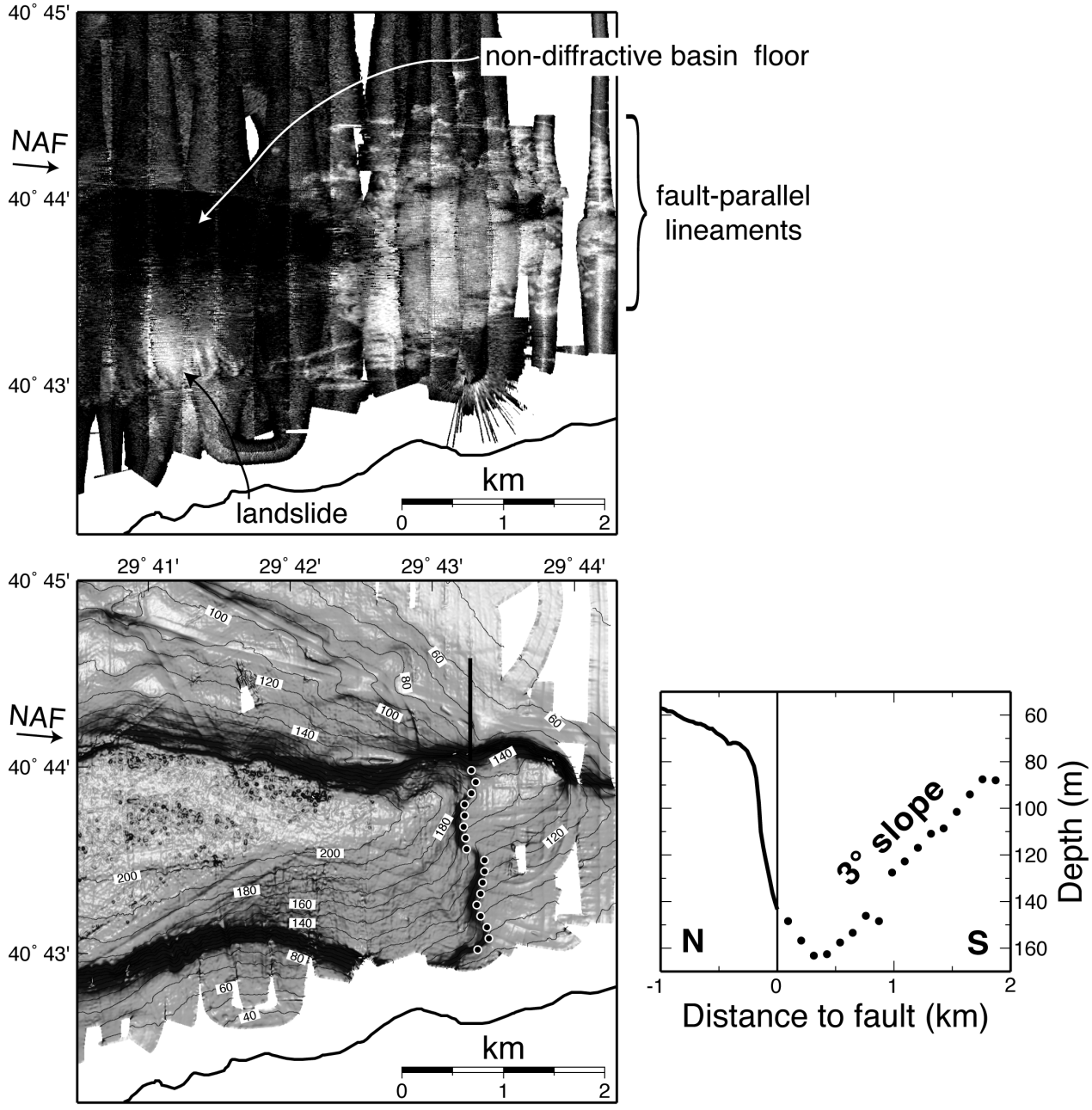

Figure 15. Detailed seafloor morphology at the eastern end of the central basin. Arrows at left point to the North Anatolian Fault (NAF). (top) Acoustic backscatter imagery; lighter shades indicate higher backscatter amplitude. The series of EW lineaments are not associated with any detectable relief and may indicate open fractures and/or mole tracks resulting from the 1999 earthquake. The patch of reflective seafloor in the SW corner of the map likely indicates a landslide. The lack of reflectivity from the basin floor may be typical of anoxic sediments. (bottom left) Seafloor gradient with 10 m depth contours overlaid; darker shading indicates steeper slopes. Dots mark the top of the paleoshelf break where it veers northward into the fault zone (see text). Solid line locates the bathymetric profiles shown at right. (bottom right) Depth of the NS striking paleoshelf break versus distance to fault (dots). Plot is extended north of the fault with bathymetric profile (solid line). Vertical exaggeration is 20. The paleoshelf break dips 3° northward into the fault plane.

defined zone [*Ito et al.*, 2002; *Karabulut et al.*, 2002; *Özalaybey et al.*, 2002] is presented as supporting evidence. Inversions of the InSAR, GPS, and teleseismic data also suggest that the North Anatolian Fault ruptured along the entire length of Izmit Gulf, with slip averaging 1–1.5 m in the western basin [*Delouis et al.*, 2000; *Reilinger et al.*, 2000a; *Wright et al.*, 2001; *Bouchon et al.*, 2002; *Feigl et al.*, 2002; *Çakir et al.*, 2003]. The lack of a clear surface

rupture in 1999 across Hersek peninsula may then be a consequence of the 7° restraining bend at that location [*Emre et al.*, 2003a].

[26] Alternative interpretations are possible. Rather than representing aftershocks that delineate the ruptured zone, seismic activity west of Hersek may indicate earthquakes triggered on the nearby fault segments by the increase in static stress [*Pinar et al.*, 2001]. For example, the dense cluster of aftershocks west of Izmit Gulf near Yalova was dominated by normal faulting [*Özalaybey et al.*, 2002; *Aktar et al.*, 2004]. The spatial resolution of the various solutions for the 1999 surface rupture derived by inversion of geophysical observables is relatively low [*Bos and Spakman*, 2003], and inversions may be equally compatible with a termination of the 1999 rupture around Hersek peninsula [*Reilinger et al.*, 2000a, 2000b]. Spatial uncertainties may be as large as 10–20 km, as indicated by the variability of the published solutions [e.g., *Bouchon et al.*, 2002; *Delouis et al.*, 2000; *Feigl et al.*, 2002; *Sekiguchi and Iwata*, 2002], and the western extent of the rupture cannot be determined from geophysical inversion alone. An alternate interpretation, in which surface slip stopped or dropped significantly east of Hersek peninsula, would account very simply for the gap in seismicity observed around 29°35′E and for the lack of surface rupture on the peninsula itself.

[27] Modern sonar systems can detect minute variations in seafloor relief and texture and a careful analysis of the data presented in this paper can bring additional constraints on the extent of the 1999 surface rupture. The multibeam and side scan sonar systems used during expeditions MARMARA2000 and MARMARA2001 routinely mapped cables, pipelines, and drag marks from ship anchors, and imaged subtle fault scarps, fractures, and mounds. Swath data for Western and Central basins reveal a seafloor that is undisturbed along the fault zone, in sharp contrast with the area within 8 km from the Golcuk land rupture.

[28] A lack of seafloor roughness along the fault zone west of Hersek peninsula is documented from several sources. Towed side-scan sonar data acquired during expedition MARMARA2000 indicate a uniformly low reflectivity across the fault trace except for some occasional anchor drag marks. Acoustic backscatter data produced from all three multibeam bathymetry systems also indicate a smooth seafloor (Figure 8). Although shaded relief renditions of the bathymetry clearly delineate the fault strands (Figure 2a), seafloor slopes measured in a direction transverse to the fault from raw multibeam echo sounder pings do not exceed 6° (Figure 16). Direct observations made across several fault strands during expedition MARMARA2001 with a towed camera (tracks located in Figure 8) indicate an undisturbed muddy substrate draping a gently sloping seafloor. Acoustic backscatter in central basin is also featureless except in three areas. Most strikingly, highly reflective seafloor occurs in the eastern part of the basin (Figure 15). A series of reflective lineaments strike subparallel to the main fault branch and cut across the depth contours. These lineaments have no detectable relief in the bathymetry and must therefore have less than 50 cm of relief. Their pattern is akin to the EW open fractures associated with lateral spreading along the southern shore of central basin after the 1999 earthquake [*Lettis et al.*, 2002; *Emre et al.*, 2003a], and our preferred interpretation is that they represent a network of open cracks or mole tracks that formed during the 1999 earthquake. High backscatter values also outline a mass wasting deposit about 1 km across, just below the southern shelf break near 29°41′E. That small slump may also have occurred during the 1999 earthquake. The third area of reflective seafloor occurs north of Hersek peninsula, where bottom currents probably keep the basement free of Holocene sediments (Figure 4). In contrast, the very low reflectivity of the basin floor (>205 m deep) indicates extreme attenuation of acoustic energy (Figure 15); similarly weak backscatter has been reported for the deep Santa Barbara basin offshore California [*Eichhubl et al.*, 2002] and may be a characteristic of anoxic mud with high gas content.

[29] Features associated with ground rupture might include open fractures, small slumps, mole tracks, and lateral spreading, all of which would roughen the seafloor and produce high acoustic backscatter. However, underwater, ground shaking may also trigger a series of events that contribute to masking the ground rupture. Disruption might be particularly prevalent for gas-charged sediments such as in the eastern and central basins, where fluidization or liquefaction would destroy rupture-related features. During an earthquake, strong ground shaking, seiche waves, or turbidites could also send fine sediments in suspension [*Marco and Agnon*, 1995; *Thunell et al.*, 1999; *Itou et al.*, 2000] and the slow settling of these sediments on the seafloor could mask the evidence for a ground rupture. However, we find it significant that, although finer sediments occur at the eastern side of Central basin [*Algan et al.*, 1999] near the area of maximum ground motion on 17 August 1999, acoustic backscatter data clearly highlight a network of fault-parallel features. If sediments were sent in suspension by seismogenic activity in 1999, their subsequent settling was not sufficient to mask the effects of the surface rupture. Altogether, the sonar data suggest that on 17 August 1999, surface slip stopped or decreased dramatically near 29°40′–42′E, about 14 km east of Hersek peninsula. It does not preclude, however, that the fault may have slipped in the lower crust by about 1 m.

[30] The estimated subsidence rate of 8 mm/yr of the southern fault block near 29°43′E could be accomplished with discrete 1–2 m vertical displacements during major earthquakes every few centuries, and it may have done so in the eastern portion of Central basin during the 1999 earthquake. Coastal subsidence, lateral spreading, and submarine landslides occurred along the southern shore of the basin between 29°37′–47′E (Figure 3c) adjacent to the extensional segment of the fault, while the northern shore was little affected [*Lettis et al.*, 2000; *Barka et al.*, 2002; *Emre et al.*, 2003a; *Rothaus et al.*, 2004]. The EW lineaments we mapped across a 2.5-km-wide zone centered on the fault east of 29°42′E suggest that lateral spreading also took place at the seafloor. The pattern of tsunami runups in the Gulf of Izmit indicates that it resulted predominantly from submarine faulting rather than landslides, requiring that dip-slip motion occurred in the central basin [*Öztürk et al.*, 2000; *Altinok et al.*, 2001; *Rothaus et al.*, 2004]. The small landslide along the steep southern margin of the basin near 29°41′E (Figure 15) could have been triggered by coseismic tilt.

[31] What may have caused the 1999 surface slip to decrease abruptly near 29°42′E remains to be determined.

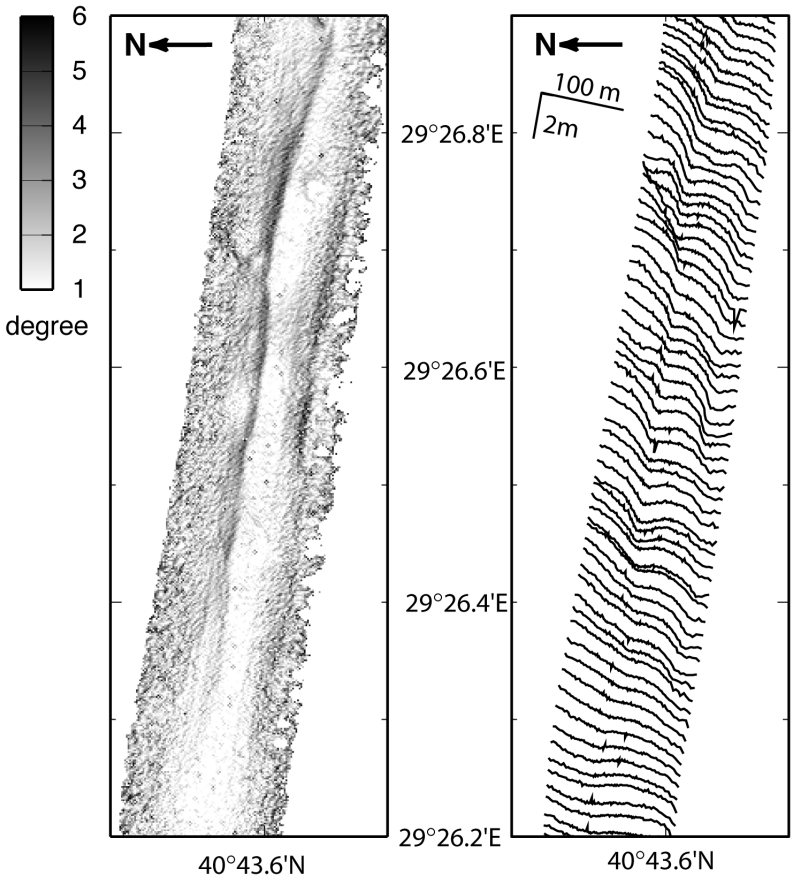

Figure 16. Raw multibeam bathymetric data illustrating subtle variations in seafloor slopes. This swath was acquired with the EM3000 system (300 kHz) parallel to the fault trace in the western basin in water depth of 63–73 m. North is to the left. (left) Seafloor slopes computed for the raw data. Slopes across the fault trace do not exceed 6°. (right) Unprocessed sonar pings provide a series of ~NS depth profiles across the fault zone. For clarity, only every fifth ping along track is plotted in its approximate geographical position. Vertical exaggeration is 30. For each ping, the average spatial sampling across track is ~1 m. Steep scarps, as might be expected from an earthquake rupture, are not visible in the raw data. While mole tracks would not be detected at this resolution, they would be expected to show in the associated backscatter (Figure 8).

On the basis of preexisting conventional bathymetric data, it was proposed that the fault described a 4–5 km releasing step over across the central basin, and that this step over could have arrested rupture propagation [*Lettis et al.*, 2002]. However, the fault describes instead a double bend between 29°40′–48′E that is roughly equivalent to a 1.3 km right stepping fault jog (Figure 3). Similar or larger fault jogs (1–4 km) did not arrest the propagation of the surface rupture in 1999 [*Harris et al.*, 2002; *Lettis et al.*, 2002], and an additional mechanism is therefore required. The North Anatolian Fault likely ruptured through Izmit Gulf during the 10 July 1894 earthquake, and much of the accumulated static stress must have been relieved at that time. Patterns of damage and aftershock from that earthquake indicate a magnitude Ms = 7.3, similar to that of the 17 August 1999 earthquake [*Ambraseys*, 2001]. However, unlike for the 1999 event, damage in 1894 was extensive on the Princes islands along the eastern shelf of the Marmara Sea (Figure 1) and on Hersek peninsula [*Ambraseys*, 2001], suggesting that the fault ruptured through the central basin and westward. The 1999 rupture may thus have encountered the "stress shadow" from the 1894 event in the central basin, where the fault would not have been quite primed for rupturing [*Harris et al.*, 2002]. If this scenario is correct, adjustments are needed to published models for static stress loading of the North Anatolian Fault beneath the Marmara Sea, and more generally, to seismic risk assessments for that region [*Stein et al.*, 1997; *Nalbant et al.*, 1998; *Hubert-Ferrari et al.*, 2000; *Parsons et al.*, 2000; *Papadimitriou et al.*, 2001; *Pinar et al.*, 2001; *Parsons*, 2004].

6. Vertical Deformation Affecting the Southern Fault Block and Correlating With Distance to Fault Bends

[32] Results presented above document a pattern of crustal deformation that can be summarized as follows. The Western and Central basins are bisected by a single, continuous right-lateral fault that strikes roughly EW. Additional transform branches are not detected, although such branches might

occur nearshore just outside the survey boundaries. Distorted shorelines and shelf breaks dating from the LGM document that vertical motion varies both in intensity and in polarity over distances of a few kilometers along strike. This deformation is asymmetric about the fault: while the southern block subsides locally at rates of 8 mm/yr, the northern block subsides or uplifts at rates an order of magnitude slower. The deepest parts of both the Western and Central basins occur along the North Anatolian Fault, on its southern side, and vertical deformation is thus clearly accommodated on its fault plane. In the central basin, this is demonstrated by the 3° tilt of the paleoshelf break toward the fault at 29°43′E, and by the progressive tilting of the turbiditic infill toward the fault. This rapid Holocene deformation is restricted to a narrow corridor: paleoshorelines and paleoshelf breaks have remained subhorizontal outside a ~2–2.5-km-wide zone on either side of the fault. In contrast, the surface fault geometry in the eastern basin resembles that of a small pull-apart basin: the EW striking 1999 surface rupture is right stepping 1.2 km to the north, delimiting a depression bounded by two facing NW striking fault segments with opposing normal throw.

[33] Along-strike variations in seafloor morphology do correlate with minor bends in the fault trace. From east to west, the fault describes a south pointing 7° bend near 29°47.5′E, a north pointing 11° bend near 29°40′E, and another south pointing 7° bend across Hersek peninsula (Figures 17a and 17b). The physiography of the fault trace suggests that the series of fault segments defined by these bends are successively under compressional regime or dilational regime. Accordingly, the presence of extensional Riedel shear west of Hersek may be favored by the slightly releasing strike of the fault relative to local plate motion; conversely, the occurrence of small folds across the fault trace in the central basin may be favored by a slightly compressional fault strike. The NW-SE fault splay in the western basin describes a releasing bend west of 29°27′E, and most likely, a restraining bend east of that longitude where it may strike ENE across Hersek peninsula and merge with the main branch in the central basin. The uplift history of the peninsula [*Alpar and Güneysu*, 1999; *Witter et al.*, 2000] and the presence of three mud volcanoes along its western shore (see section 3.1) are compatible with a slightly compressional regime associated with the southern fault splay. The 1999 surface rupture strikes ~N090° where it plunges beneath Izmit Gulf and where it resurfaces near Golcuk; at both locations, it displays nil or insignificant throws, compatible with pure strike-slip motion [*Lettis et al.*, 2000; *Emre et al.*, 2003a]. Hence the motion vector across the North Anatolian Fault through Izmit Gulf may strike close to N090°E, a value intermediate between the strikes of the compressive segment (86°) and dilational segments (93°–97°) (Figures 17a and 17b). This orientation is also intermediate between the orientations predicted for the Euler poles derived from interseismic GPS measurements (N075°–078°E [*McClusky et al.*, 2000]) and the North Anatolian Fault geometry across Marmara Sea (N097°–100°E [*Le Pichon et al.*, 2003]). Although N090° is counterclockwise to GPS velocities measured south of Izmit Gulf by *McClusky et al.* [2000] (N095° to N097; Figure 1), it fits within their 95% confidence interval.

[34] The minor bends of the fault through Izmit Gulf also correlate with along-strike variations in seafloor depths (Figure 17d). Maximum or minimum depths measured south of, and within 1 km from the fault trace vary monotonically from fault bend to fault bend, reaching some extremum near each bend. Depth increases westward along the two dilational fault segments, and the opposite trend applies along the compressive segment (29°40′E to Hersek).

[35] Similarly, minor bends in the fault trace correlate with cumulative uplift or subsidence over the past several millennia (Figure 17c). Indeed, relative changes in elevation across the fault for areas that would have been maintained flat by erosional or depositional processes during the LGM provide a direct estimate of vertical displacement since that time. Such areas include the shelves that developed around the paleolake in the central basin and now lay deeper than ~65 m (see section 3.2). Others include shallow areas that were subaerially exposed during the last Glacial and now lay above 87 m west of Hersek and above 65 m east of Hersek (see sections 3.1 and 3.2). These surfaces would have been rapidly submerged below wave base during the last marine transgression between 10–14 ka [*Fairbanks.*, 1989], and the fault escarpments cutting across them likely record vertical displacements that have accumulated since then. East of Hersek on the paleoshelves, the thickness of the Holocene drape does not vary significantly across the fault trace and the vertical displacement in Figure 17c have been estimated directly from the bathymetry. West of Hersek, the thickness of the Holocene drape does vary significantly across the fault (section 3.1 and Figure 5). Cumulative throws in Figure 17c are therefore estimated from the map of the Holocene basement by measuring the maximum depth variations within 1 km from the fault trace. The resulting curve for cumulative throw is incomplete but the observed trends match those of the bathymetry south of the fault. Where measurable, variations in cumulative throw over the past 10–14 kyr are roughly half the bathymetric variations.

[36] These simple correlations suggest that even with the smoothing effect of mass wasting and other sedimentary processes, water depth alone can be a good indicator of recent tectonics. The next section presents a self-consistent structural model that accounts for these correlations and the physiography of Izmit Gulf.

7. Model for Vertical Deformations Along Transform Faults: Primarily Controlled by Fault Dip and Fault Bends

[37] The basins that define the Marmara Sea and the Gulf of Izmit are commonly viewed as a series of negative flower structures [*Aksu et al.*, 2000; *Gökasan et al.*, 2001; *Alpar and Yaltirak*, 2002] or as a series of pull-apart basins [*Barka and Kadinsky-Cade*, 1988; *Wong et al.*, 1995; *Armijo et al.*, 2002; *Lettis et al.*, 2002]. Models for negative flower structures propose that at extensional jogs, the fault branches upward into a series of subparallel faults that accommodate both strike-slip and normal components [*Harding*, 1985]. Models for pull-apart basins propose that at extensional offsets along transform faults, slip is distributed between two overlapping strike-slip segments and some intervening normal faults [*Rodgers*, 1980; *Mann et al.*, 1983]. A recent model advo-

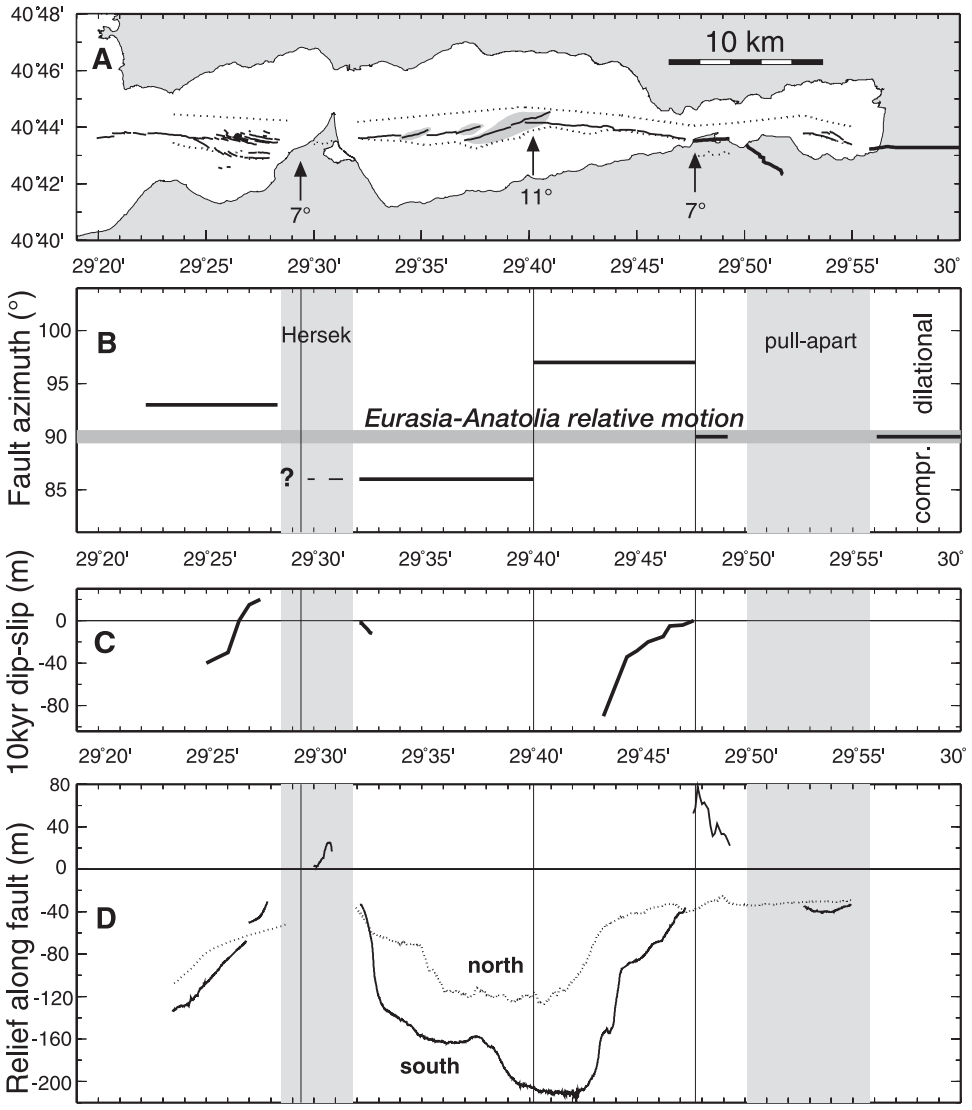

Figure 17. Fault strike and vertical deformation. (a) Geometry of the North Anatolian Fault across Izmit Gulf. Thick lines indicate the 1999 surface rupture, and arrows point to fault bends. Thin lines indicate the submarine trace. Dotted lines locate the two depth profiles shown in Figure 17d. (b) Mean azimuth of the fault segments delimited by fault bends versus longitude. A relative plate motion of 89°–91° (shaded areas) would be compatible with a morphological indicator of transpression, transtension, or pure strike slip along each segment (see text). (c) Differential topography across the fault for the shelf areas that were exposed during the Last Glacial Maximum (see text). Negative (positive) values indicate where the southern block subsided (uplifted). Measurements west of Hersek peninsula are taken from the map of the base Holocene in Figure 5b. The Holocene drape is relatively thin over the shelves east of Hersek, and measurements are taken directly from the bathymetry. (d) Maximum relief within 1 km from the fault trace versus longitude (solid line, south side; dotted line, north side). Measurements are taken from multibeam bathymetric data (this paper) and altimetry data (NASA Shutte Radar Topography Mission).

cates instead that the Marmara basins formed during an initial extensional phase and became mostly inactive after the North Anatolian Fault cleaned its course and cut across them [*Le Pichon et al.*, 2001; *Kusçu et al.*, 2002; *Demirbag et al.*, 2003; *Rangin et al.*, 2004].

[38] Results documented in this paper challenge the applicability of the above models to Izmit Gulf. First, multibeam bathymetric data highlight a fault that is mostly throughgoing across Izmit Gulf and, except for the eastern basin, there is no evidence for active normal faults (Figures 2 and 3). Second, the 80 m of Holocene subsidence of the southern fault block at the east end of the central basin (Figure 15) and the progressive tilting of the Holocene strata toward the North Anatolian Fault (Figure 12, line I-44) indicate that rapid vertical motion is accommodated by dip slip on this throughgoing transform fault. We thus propose an alternate model in which asymmetric basins and ridges develop where a continental transform meets two conditions: its fault plane is not quite vertical, and its strike deviates locally from relative plate motion. With such fault

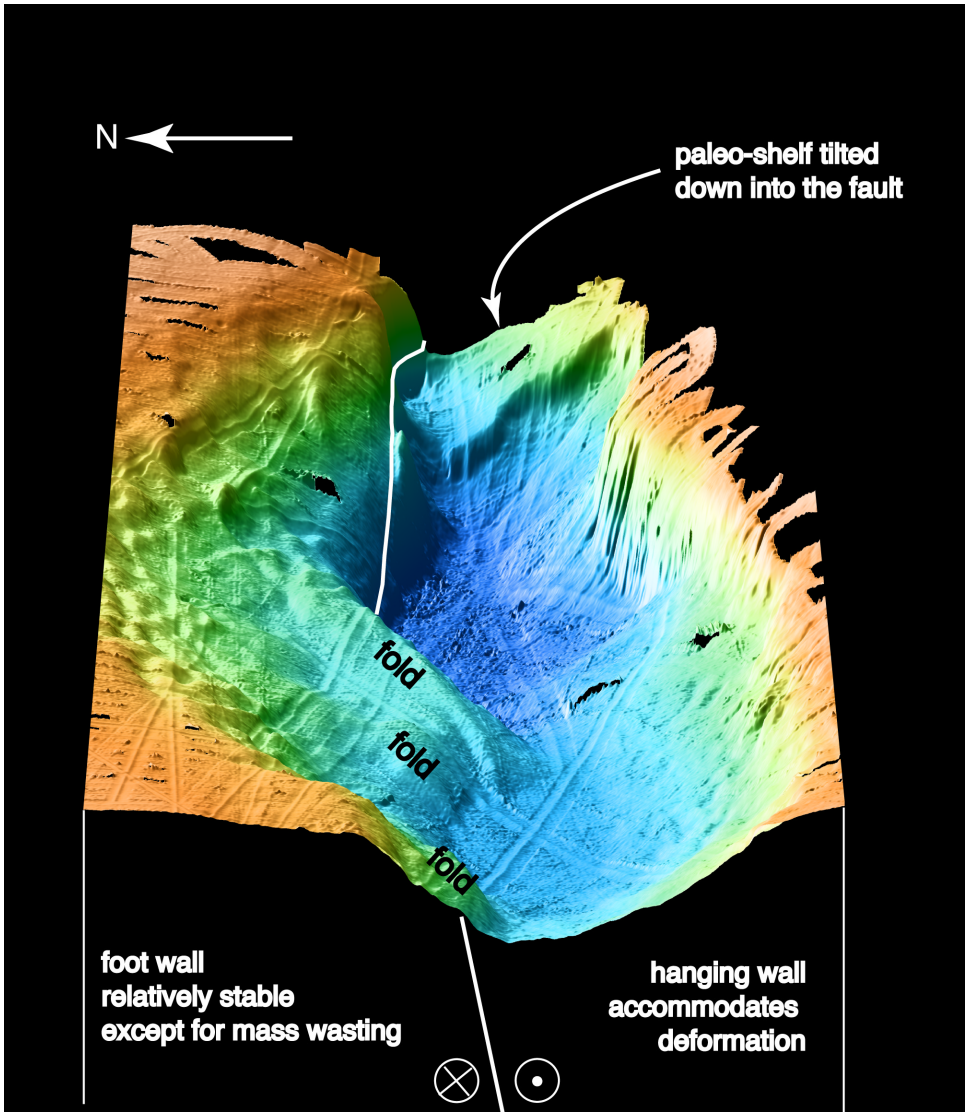

Figure 18. Three-dimensional view of the central basin, looking toward the east. View area is 6.5 km across and 14 km long, and vertical exaggeration is 7. The white line marks the trace of the North Anatolian Fault. A subsurface fault geometry that could explain the rapid Holocene subsidence of the southern fault block is sketched in the foreground.

geometry, vertical motion will be accommodated by subsidence or uplift of the hanging wall block in the transform fault plane, rather than by slip partitioning on secondary normal faults or reverse faults. In contrast, the footwall block will offer a stable slip surface and be largely unaffected by vertical tectonics. That model also fits the pattern of vertical deformation at a 17° bend of the North Anatolian Fault, at the western side of the Marmara Sea: there, major vertical deformations north of the fault are proposed to reflect a 50°–80°dip of the fault toward the north [*Okay et al.*, 2004; *Seeber et al.*, 2004]. In the case of a steeply dipping fault striking obliquely to relative motion, a small amount of cumulative horizontal slip could result in large vertical motion of the hanging wall block.

[39] Source parameters for the 1999 Izmit earthquake indicate a near-vertical fault plane, and are compatible with a steep dip (>80°) to the south [*Li et al.*, 2002]. Aftershocks epicenters through the central and western basins in Izmit Gulf are mapping 1 to 2 km south of the surface fault trace [*Ito et al.*, 2002; *Özalaybey et al.*, 2002]. This observation is also consistent with a steeply southward dipping fault plane, although admittedly, uncertainties in the seismic structure of the crust could contribute to mislocating the aftershocks by a few kilometers. Assuming the North Anatolian Fault dips 85°–88° southward through Izmit Gulf, minor deviations of its azimuth from plate motion could locally produce large vertical displacement of the southern fault block. In particular, a steep dip could account for the rapid subsidence (8 mm/yr) documented in the central basin, adjacent to the 7° releasing trend of the fault (Figure 18). Adjusting for a sedimentation rate of about 5 mm/yr at the basin floor [*McHugh et al.*, 2003], this rapid subsidence rate implies that the 140 m of vertical relief in the central basin could have developed in as little as a few 100,000 years.

[40] A youthful origin for the basins in Izmit Gulf appears incompatible with the older age of the North Anatolian

Fault in the Marmara region, with estimates ranging between 5 Myr and 7 Myr [*Sengör*, 1979; *Görür et al.*, 1997; *Armijo et al.*, 1999]. Nonetheless, the present geometry of the North Anatolian Fault across the Marmara Sea is thought to have developed recently, with estimate ranging between 200,000 years [*Le Pichon et al.*, 2003] and 1.2–2 Myr [*Emre et al.*, 1998; *Okay et al.*, 2004; *Seeber et al.*, 2004]. If confirmed, the young age of the basins in Izmit Gulf could reflect the ephemeral nature of small (<4 km) step overs and fault bends, and their possible migration or spawning along the fault trace in response to inherited structural complexities.

[41] A steep dip of the fault plane not only could account for the asymmetry and rapidity of the vertical deformation, but also for the reversal of the deformation trend (uplift or subsidence) at successive fault bends (Figures 17b and 17c). The vertical deformation of the southern (hanging wall) block varies monotonically with distance from each fault bend where a new deformation style initiates: in other words, the uplift or subsidence of the southern block is getting more pronounced westward as the southern block moves away from each bend. The reason for this monotonic variation from bend to bend is unclear, but may indicate that a deformation style does not become established instantaneously as the plate passes around a bend. Instead, the full impact of the new stress regime may be realized some distance away from a bend.

[42] Whether the North Anatolian Fault dips indeed steeply to the south through Izmit Gulf should be revealed in the next large earthquake this century. That future earthquake will also test whether slip from the 1999 earthquake did drop abruptly west of Golcuk (see section 5): if it did, the area around Hersek peninsula and the western basin should be strongly affected by the next earthquake. On the other hand, on the basis of the patterns of Holocene deformation, little vertical deformation should affect the shorelines of the western basin, as they are located more than 3 km from the fault trace. In the area surrounding Hersek peninsula, mud volcanoes may become activated and liquefaction and sediment fluidization should be expected, as may have been the case in 1894 (see section 3 and 5).

8. Conclusions

[43] 1. The North Anatolian Fault generally follows the axis of Izmit Gulf, describing a few minor bends along its length.

[44] 2. Paleoshorelines, paleoshelf breaks, and shelf areas that were subaerially exposed during the Last Glacial Age provide key markers to evaluate vertical deformation in the Western (Darica) and Central (Karamürsel) basins. The northern fault block appears relatively stable, while the southern fault block locally subsides very rapidly, at rates of up to 8 mm/yr.

[45] 3. Holocene vertical deformation of the southern block varies monotonically from fault bend to fault bend. This correlation can be explained if the plane of the North Anatolian Fault is dipping steeply to the south, accommodating oblique slip motion in its fault plane. Such model does not require the existence of subsidiary normal or reverse faults that accommodate significant plate boundary strain, and may imply a young age for the formation of Izmit Gulf (a few 100,000 years).

[46] 4. Backscatter imagery suggest that the surface slip from the 17 August 1999 earthquake stopped (or decreased sharply) 7 km west of Golcuk, in the central (Karamürsel) basin. This observation is compatible with the 10 July 1894 earthquake having ruptured the fault through western Izmit Gulf.

[47] 5. Sedimentary features such as mass wasting, fluidization structures, and mud volcanoes occur along the fault trace, suggesting that large earthquakes in the Marmara Sea are accompanied by widespread expulsion of fluid and/or gas.

[48] **Acknowledgments.** We thank the Turkish Council for Technical and Scientific Research (TÜBITAK) and the General Directorate of Mineral Research and Exploration (MTA) for their assistance and logistic support of this project, as well as the Turkish Department of Navigation, Hydrography and Oceanography (SHOD) for providing their 1999 multibeam bathymetry data. We are grateful to the captains and crews of the *R/V Odin Finder* and of the *R/V Urania* for their professionalism and dedication. The technical expertise of Emanuele Bartolini at Geological Assistance Services, S.A., and of Alessandro Blasi at the Institute of Marine Sciences in Bologna guaranteed the success of the two surveys. The scientific parties for the two expeditions also included Martina Busetti, Lucilla Capotondi, Kadir Eris, Paola Fabretti, E. J. Fielding, Caner Imren, Hulya Kurt, Marco Ligi, Alessandro Magagnoli, Gabrielle Marozzi, Nilgün Okay, Naside Ozer, Daniella Penitenti, Kerim Sarikavak, Giorgio Serpi, and Bugser Tok. Emin Demirbag at Istanbul Technical University kindly provided us with available digital data for the area. We thank Amotz Agnon, Christopher Sorlien, and an anonymous reviewer for their thoughtful reviews and constructive criticisms of the manuscript. Christopher Sorlien reprocessed the chirp data displayed in Figures 12 and 14. Ata Suanda assisted with the interpretation of the chirp data during a summer internship at LDEO. James Dolan contributed invaluable ideas at the initial phase of this project. Figures have been prepared with the free software GMT [*Wessel and Smith*, 1998]. NATO Collaborative Linkage grant 976826 provided seed funding and made this international collaboration possible. Data acquisition and analysis have been jointly financed by U.S. National Science Foundation grants OCE-0096668 and OCE-0222285, the Italian National Research Council (CNR), TÜBITAK, and Lamont-Doherty Earth Observatory. Lamont-Doherty contribution 6766.

References

Aksu, A. E., R. N. Hiscott, and D. Yasar (1999), Oscillating Quaternary water levels of the Marmara Sea and vigorous outflow into the Aegean Sea from the Marmara Sea–Black Sea drainage corridor, *Mar. Geol.*, *153*, 275–302.

Aksu, A. E., T. J. Calon, R. N. Hiscott, and D. Yasar (2000), Anatomy of the North Anatolian Fault zone in the Marmara sea, western Turkey: Extensional basins above a continental transform, *GSA Today*, *10*, 3–7.

Aktar, M., S. Özalaybey, M. Ergin, H. Karabulut, M.-P. Bouin, C. Tapirdamaz, F. Biçmen, A. Yörük, and M. Bouchon (2004), Spatial variation of aftershock activity across the rupture zone of the 17 August 1999 Izmit earthquake, Turkey, *Tectonophysics*, *391*, 325–334.

Algan, O., H. Altinok, and H. Yüce (1999), Seasonal variation of suspended particulate matter in two-layered Izmit bay, Turkey, *Estuarine Coastal Shelf Sci.*, *49*, 235–250.

Alpar, B. (1999), Underwater signature of the Kocaeli earthquake (August 17th 1999), *Turkish J. Marine Sciences*, *5*, 111–130.

Alpar, B., and A. C. Güneysu (1999), Evolution of the Hersek delta (Izmit Bay), *Turk. J. Mar. Sci.*, *5*, 57–74.

Alpar, B., and C. Yaltirak (2002), Characteristic features of the North Anatolian Fault in the eastern Marmara region and its tectonic evolution, *Mar. Geol.*, *190*, 329–350.

Altinok, Y., S. Tinti, B. Alpar, A. C. Yalçiner, S. Ersoy, E. Bortolucci, and A. Armigliato (2001), The tsunami of August 17, 1999 in Izmit Bay, Turkey, *Nat. Hazards*, *24*, 133–146.

Ambraseys, N. N. (2001), The earthquake of 10 July 1894 in the Gulf of Izmit (Turkey) and its relation to the earthquake of 17 August 1999, *J. Seismol.*, *5*, 117–128.

Armijo, R., B. Meyer, A. Hubert, and A. A. Barka (1999), Westward propagation of the north Anatolian Fault into the northern Aegean: Timing and kinematics, *Geology*, *27*, 267–270.

Armijo, R., B. Meyer, S. Navarro, G. C. P. King, and A. A. Barka (2002), Asymmetric slip partitioning in the Sea of Marmara pull-apart: A clue to propagation processes of the North Anatolian Fault?, *Terra Nova*, *14*, 80–86.

Barka, A. A. (1996), Slip distribution along the North Anatolian Fault associated with the large earthquakes of the period 1939 to 1967, *Bull. Seismol. Soc. Am.*, *86*, 1238–1254.

Barka, A. A. (1999), The 17 August 1999 Izmit earthquake, *Science*, *285*, 1858–1859.

Barka, A. A. (2002), The surface rupture and slip distribution of the 17 August 1999 Izmit earthquake (*M* 7.4), North Anatolian Fault, *Bull. Seismol. Soc. Am.*, *92*, 43–60.

Barka, A. A., and K. Kadinsky-Cade (1988), Strike-slip fault geometry in Turkey and its influence on earthquake activity, *Tectonics*, *7*, 663–684.

Barka, A. A., and I. Kusçu (1996), Extents of the North Anatolian Fault in the Izmit, Gemlik and Bandirma bays, *Turk. J. Mar. Sci.*, *2*, 93–106.

Bos, A. G., and W. Spakman (2003), The resolving power of coseismic surface displacement data for fault slip distribution at depth, *Geophys. Res. Lett.*, *30*(21), 2110, doi:10.1029/2003GL017946.

Bouchon, M., M. N. Toksöz, H. Karabulut, M.-P. Bouin, M. Dietrich, M. Aktar, and M. Edie (2002), Space and time evolution of rupture and faulting during the 1999 Izmit (Turkey) earthquake, *Bull. Seismol. Soc. Am.*, *92*, 256–266.

Çagatay, M. N., N. Görür, O. Algan, C. J. Eastoe, A. Tchapalyga, D. Ongan, T. Kuhn, and I. Kusçu (2000), Late Glacial-Holocene palaeoceanography of the Sea of Marmara: Timing of connections with the Mediterranean and the Black Seas, *Mar. Geol.*, *167*, 191–206.

Çagatay, M. N., N. Görür, A. Polonia, E. Demirbag, M. Sakinç, M. H. Cormier, L. Capotondi, C. M. G. McHugh, Ö. Emre, and K. Eris (2003), Sea-level changes and depositional environments in the Izmit Gulf, eastern Marmara Sea, during the late glacial–Holocene period, *Mar. Geol.*, *202*, 159–173.

Çakir, Z., J.-B. de Chabalier, R. Armijo, B. Meyer, A. A. Barka, and G. Peltzer (2003), Coseismic and early post-seismic slip associated with the 1999 Izmit earthquake (Turkey), from SAR interferometry and tectonic field observations, *Geophys. J. Int.*, *155*, 93–110.

Caress, D. W., and D. N. Chayes (2002), Processing, archiving, and disseminating large swath mapping datasets using MB-system, *Eos Trans. American Geophysical Union*, *83*(47), Fall Meet. Suppl., Abstract OS61C-07.

Chapron, E., P. Van Rensbergen, M. De Batist, C. Beck, and J. P. Henriet (2004), Fluid-escape features as a precursor of a large sublacustrine sediment slide in Lake Le Bourget, NW Alps, France, *Terra Nova*, *16*, 305–311.

Çifçi, G., D. Dondurur, and M. Ergun (2003), Deep and shallow structures of large pockmarks in the Turkish shelf, eastern Black Sea, *Geo Mar. Lett.*, *23*, 311–322.

Clifton, H. E., H. G. Greene, G. W. Moore, and R. L. Phillips (1971), Methane seep off Malibu Point following the San Fernando earthquake, in *The San Fernando, California, Earthquake of February 9, 1971: A Preliminary Report Published Jointly by the U.S. Geological Survey and the National Oceanic and Atmospheric Administration*, *U.S. Geol. Surv. Prof. Pap.*, *733*, 112–116.

Davies, R. J. (2003), Kilometer-scale fluidization structures formed during early burial of a deep-water slope channel on the Niger Delta, *Geology*, *31*, 949–952.

Delouis, B., P. Lundgren, J. Salichon, and D. Giardini (2000), Joint inversion of InSAR and teleseismic data for the slip history of the 1999 Izmit (Turkey) earthquake, *Geophys. Res. Lett.*, *27*, 3389–3392.

Demirbag, E., C. Rangin, X. Le Pichon, and A. M. C. Sengör (2003), Investigation of the tectonics of the Main Marmara Fault by means of deep-towed seismic data, *Tectonophysics*, *361*, 1–19.

Dimitrov, L. I. (2002), Mud volcanoes: The most important pathway for degassing deeply buried sediments, *Earth Sci. Rev.*, *59*, 49–76.

Eichhubl, P., H. G. Greene, and N. Mahler (2002), Physiography of an active transpressive margin basin: High-resolution bathymetry of the Santa Barbara basin, southern California continental borderland, *Mar. Geol.*, *184*, 95–120.

Emre, Ö., T. Erkal, A. Tchapalyga, N. Kazanci, M. Keçer, and E. Ünay (1998), Neogene-Quaternary evolution of the eastern Marmara region, northwest Turkey, *Bull. Miner. Res. Explor.*, *120*, 119–145.

Emre, Ö., Y. Awata, and T. Y. Duman (2003a), *Surface Rupture Associated With the 17 August 1999 Izmit Earthquake*, 280 pp., Gen. Dir. of Miner. Res. and Explor., Ankara.

Emre, Ö., et al. (2003b), The retraining Hersek bend: Is it a barrier to rupture propagation for the 1999 Izmit earthquake?, paper presented at International Workshop on the North Anatolian and East Anatolian and Dead Sea Fault Systems, Middle East Tech. Univ., Ankara, 31 Aug. to 12 Sept.

Fairbanks, R. G. (1989), A 17,000 year glacioeustatic sea-level record: Influence of glacial melting rates on the Younger Dryas event and deep-ocean circulation, *Nature*, *342*, 637–742.

Feigl, K. L., F. Sarti, H. Vadon, S. C. McClusky, S. Ergintav, P. Durand, R. Bürgmann, A. Rigo, D. Massonnet, and R. E. Reilinger (2002), Estimating slip distribution for the Izmit mainshock from coseismic GPS, RADARSAT, ERS-1, and SPOT measurements, *Bull. Seismol. Soc. Am.*, *92*, 138–160.

Field, M. E., and A. E. Jennings (1987), Seafloor gas seeps triggered by a northern California earthquake, *Mar. Geol.*, *77*, 39–51.

Gardner, J. V., L. A. Mayer, and J. E. H. Clarke (2000), Morphology and processes in Lake Tahoe (California-Nevada), *GSA Bull.*, *112*, 735–746.

Gardner, J. V., P. Dartnell, L. A. Mayer, and J. E. Hughes Clarke (2003), Geomorphology, acoustic backscatter, and processes in Santa Monica Bay from multibeam mapping, *Mar. Environ. Res.*, *56*, 15–46.

Griboulard, R., C. Bobier, J. C. Faugères, and G. Vernette (1991), Clay diapiric structures within the strike-slip margin of the southern leg of the Barbados prism, *Tectonophysics*, *192*, 383–387.

Gökasan, E., B. Alpar, C. Gazioglu, Z. Y. Yücel, B. Tok, E. Dogan, and A. C. Güneysu (2001), Active tectonics of the Izmit Gulf (NE Marmara Sea): From high resolution seismic and multi-beam bathymetry data, *Mar. Geol.*, *175*, 273–296.

Görür, N., M. N. Çagatay, M. Sakinç, M. Sümengen, K. Sentürk, C. Yaltirak, and A. Tchapalyga (1997), Origin of the Sea of Marmara as deduced from Neogene to Quaternary paleogeographic evolution of its frame, *Int. Geol. Rev.*, *39*, 342–352.

Görür, N., G. A. Papadopoulos, and N. Okay (2002), Preface, in *Proceedings of the NATO Seminar on Integration of Earth Science Research on the Turkish and Greek 1999 Earthquakes and Needs for Future Cooperative Research, Istanbul, 14–17 May 2000*, edited by N. Görür, G. A. Papadopoulos, and N. Okay, pp. vii–viii, Springer, New York.

Harding, T. P. (1985), Seismic characteristics and identification of negative flower structures, positive flower structures, and positive structural inversion, *AAPG Bull.*, *69*, 582–600.

Harris, R. A., J. F. Dolan, R. D. Hartleb, and S. M. Day (2002), The 1999 Izmit, Turkey, earthquake: A 3D dynamic stress transfer model for intraearthquake triggering, *Bull. Seismol. Soc. Am.*, *92*, 245–255.

Hasiotis, T., G. Papatheodorou, N. Kastanos, and G. Ferentinos (1996), A pockmark field in the Patras Gulf (Greece) and its activation during the 14/7/93 seismic event, *Mar. Geol.*, *130*, 333–344.

Hieke, W. (2004), The August 27, 1886 earthquake in Messenia (Peloponnesus) and reported flames over the Ionian Sea: A Mediterranean ridge gas escape event? Mar, *Geol.*, *207*, 259–265.

Hubert-Ferrari, A., A. A. Barka, E. Jacques, S. S. Nalbant, B. Meyer, R. Armijo, P. Tapponier, and G. C. P. King (2000), Seismic hazard in the Marmara Sea region following the 17 August 1999 Izmit earthquake, *Nature*, *404*, 269–273.

Hughen, C., J. Mascle, E. Chaumillon, A. Kopf, J. M. Woodside, and T. A. C. Zitter (2004), Structural setting and tectonic control of mud volcanoes from the central Mediterranean Ridge (eastern Mediterranean), *Mar. Geol.*, *209*, 245–263.

Ito, A., S. B. Üçer, S. Baris, A. Nakamura, Y. Honkura, T. Kono, S. Hori, A. Hasewaga, R. Pektas, and A. M. Isikara (2002), Aftershock activity of the 1999 Izmit, Turkey, earthquake, revealed from microearthquake observations, *Bull. Seismol. Soc. Am.*, *92*, 418–427.

Itou, M., I. Matsumara, and S. Noriki (2000), A large flux of particulate matter in the deep Japan Trench observed just after the 1994 Sanriku-Oki earthquake, *Deep Sea Res., Part I*, *47*, 1987–1998.

Karabulut, H., M. P. Bouin, M. Bouchon, M. Dietrich, C. Cornou, and M. Aktar (2002), The seismicity in the eastern Marmara Sea after the 17 August 1999 Izmit earthquake, *Bull. Seismol. Soc. Am.*, *92*, 387–393.

Kelley, J. T., S. M. Dickson, D. F. Belknap, W. A. Barnhardt, and M. Henderson (1994), Giant sea-bed pockmarks: Evidence for gas escape from Belfast Bay, Maine, *Geology*, *22*, 59–62.

Kopf, A. J. (2002), Significance of mud volcanism, *Rev. Geophys.*, *40*(2), 1005, doi:10.1029/2000RG000093.

Kopf, A. J. (2003), Global methane emission through mud volcanoes and its past and present impact on the Earth's climate, *Int. J. Earth Sci.*, *92*, 806–816.

Kusçu, I., M. Okamura, H. Matsuoka, and Y. Awata (2002), Active faults in the Gulf of Izmit on the North Anatolian Fault, NW Turkey: A high-resolution shallow seismic study, *Mar. Geol.*, *190*, 421–443.

Lajoie, K. R. (1986), Coastal tectonics, in *Active Tectonics*, edited by R. E. Wallace, pp. 95–124, Natl. Acad., Washington, D. C.

Le Pichon, X., et al. (2001), The active Main Marmara Fault, *Earth Planet. Sci. Lett.*, *192*, 595–616.

Le Pichon, X., N. Chamot-Rooke, C. Rangin, and A. M. C. Sengör (2003), The North Anatolian Fault in the Sea of Marmara, *J. Geophys. Res.*, *108*(B4), 2179, doi:10.1029/2002JB001862.

Lettis, W. R., J. Bachhuber, A. A. Barka, R. C. Witter, and C. Brankman (2000), Surface fault rupture and segmentation during the Kocaeli earthquake, in *The 1999 Izmit and Düzce Earthquakes: Preliminary Results*, edited by A. A. Barka et al., pp. 31–54, Istanbul Tech. Univ., Istanbul, Turkey.

Lettis, W. R., J. Bachhuber, R. C. Witter, C. Brankman, C. E. Randolph, A. A. Barka, W. D. Page, and A. Kaya (2002), Influence of releasing step-overs on surface fault rupture and fault segmentation: Examples from the 17 August 1999 Izmit earthquake on the North Anatolian Fault, Turkey, *Bull. Seismol. Soc. Am.*, *92*, 19–42.

Li, X., V. F. Cormier, and M. N. Toksöz (2002), Complex source process of the 17 August 1999 Izmit, Turkey, earthquake, *Bull. Seismol. Soc. Am.*, *92*, 267–277.

Mann, P., M. R. Hempton, D. C. Bradley, and K. Burke (1983), Development of pull-apart basins, *J. Geol.*, *91*, 529–554.

Marco, S., and A. Agnon (1995), Prehistoric earthquake deformations near Masada, Dead Sea graben, *Geology*, *23*, 695–698.

McClusky, S. C., et al. (2000), Global Positioning System constraints on plate kinematics and dynamics in the eastern Mediterranean and Caucasus, *J. Geophys. Res.*, *105*, 5695–5719.

McHugh, C. M. G., M.-H. Cormier, L. Seeber, M. N. Çagatay, G. Losfezki, L. Capotondi, and A. Polonia (2003), Earthquake geology along the North Anatolian Fault zone in the Marmara Sea, *Geophys. Res. Abstr.*, *5*, abstract 07478.

Morgan, L. A., et al. (2003), Exploration and discovery in Yellowstone Lake: Results from high-resolution sonar imaging, seismic reflection profiling, and submersible studies, *J. Volcanol. Geotherm. Res.*, *122*, 221–242.

Nalbant, S. S., A. Hubert, and G. C. P. King (1998), Stress coupling between earthquakes in northwest Turkey and the North Aegean Sea, *J. Geophys. Res.*, *103*, 24,469–24,486.

Okay, A. I., O. Tüysüz, and S. Kaya (2004), From transpression to transtension: Changes in morphology and structure around a bend on the North Anatolian Fault in the Marmara region, *Tectonophysics*, *391*, 259–282.

Özalaybey, S., M. Ergin, M. Aktar, C. Tapirdamaz, F. Biçmen, and A. Yörük (2002), The 1999 Izmit earthquake sequence in Turkey: Seismological and tectonic aspects, *Bull. Seismol. Soc. Am.*, *92*, 376–386.

Öztürk, H., H. Koral, and E. L. Geist (2000), Intra-basinal water movements induced by faulting: The August 17, 1999, Gölcük (Izmit Bay) earthquake (M_w = 7. 4), *Mar. Geol.*, *170*, 263–270.

Papadimitriou, E. E., V. G. Karakostas, and B. C. Papazachos (2001), Rupture zones in the area of the 17.08.99 Izmit (NW Turkey) large earthquake (*Mw* 7.4) and stress changes caused by its generation, *J. Seismol.*, *5*, 269–276.

Parsons, T. (2004), Recalculated probability of $M \geq 7$ earthquakes beneath the Sea of Marmara, Turkey, *J. Geophys. Res.*, *109*, B05304, doi:10.1029/2003JB002667.

Parsons, T., S. Toda, R. S. Stein, A. A. Barka, and J. H. Dieterich (2000), Heightened odds of large earthquakes near Istanbul: An interaction-based probability calculation, *Science*, *288*, 661–665.

Pinar, A., Y. Honkura, and K. Kuge (2001), Seismic activity triggered by the 1999 Izmit earthquake and its implications for the assessment of future seismic risk, *Geophys. J. Int.*, *146*, F1–F7.

Polonia, A., et al. (2002), Exploring submarine earthquake geology in the Marmara Sea, *Eos Trans. American Geophysical Union*, *83*(21), 235, 235–236.

Polonia, A., et al. (2004), Holocene slip rate of the North Anatolian Fault beneath the Sea of Marmara, *Earth Planet. Sci. Lett.*, *227*, 411–426.

Rangin, C., X. Le Pichon, E. Demirbag, and C. Imren (2004), Strain localization in the Sea of Marmara: Propagation of the North Anatolian Fault in a now inactive pull-apart, *Tectonics*, *23*, TC2014, doi:10.1029/2002TC001437.

Reilinger, R. E., et al. (2000a), Coseismic and postseismic fault slip for the 17 August 1999, *M* = 7.5, Izmit, Turkey earthquake, *Science*, *289*, 1519–1524.

Reilinger, R. E., M. N. Toksöz, S. C. McClusky, and A. A. Barka (2000b), 1999 Izmit, Turkey earthquake was no surprise, *GSA Today*, *10*, 1–6.

Rodgers, D. A. (1980), Analysis of pull-apart basin development produced by en-echelon strike-slip faults, in *Sedimentation in Oblique-Slip Mobile Zones*, *Spec. Publ. of Int. Assoc. of Sedimentol.*, vol. 4, edited by P. Ballance and H. G. Readings, pp. 27–41, Blackwell Sci., Malden, Mass.

Rothaus, R. M., E. Reinhardt, and J. Noller (2004), Regional considerations of coastline change, tsunami damage and recovery along the southern coast of the Bay of Izmit (the Kocaeli (Turkey) earthquake of 17 August 1999), *Nat. Hazards*, *31*, 233–252.

Ryan, W. B. F., W. C. Pitman, C. O. Major, K. Shimkus, V. Moskalenko, G. A. Jones, P. Dimitrov, N. Görür, M. Sakinç, and H. Yüce (1997), An abrupt drowning of the Black Sea shelf, *Mar. Geol.*, *138*, 119–126.

Seeber, L., Ö. Emre, M.-H. Cormier, C. C. Sorlien, C. M. G. McHugh, A. Polonia, N. Özer, M. N. Çagatay, and the team of the 2000 R/V *Urania* cruise in the Marmara Sea (2004), Uplift and subsidence from oblique slip: The Ganos-Marmara bend of the North Anatolian transform, western Turkey, *Tectonophysics*, *391*, 239–258.

Sekiguchi, H., and T. Iwata (2002), Rupture process of the 1999 Kocaeli, Turkey, earthquake estimated from strong-motion waveforms, *Bull. Seismol. Soc. Am.*, *92*, 300–311.

Sengör, A. M. C. (1979), The North Anatolian transform fault: Its age, offset and tectonic significance, *J. Geol. Soc. London*, *136*, 269–282.

Sengör, A. M. C., N. Görür, and F. Saroglu (1985), Strike-slip faulting and related basin formation in zones of tectonic escape: Turkey as a case study, in *Strike-Slip Deformation, Basin Formation, and Sedimentation*, edited by K. T. Biddle and N. Christie-Blick, pp. 227–264, Soc. of Econ. Paleontol. and Mineral., Tulsa, Okla.

Slater, R. A., D. S. Gorsline, R. L. Kolpack, and G. I. Shiller (2002), Postglacial sediments of the Californian shelf from Cape San Martin to the US-Mexico border, *Quat. Int.*, *92*, 45–61.

Smith, A. D., T. Taymaz, F. Y. Oktay, H. Yüce, B. Alpar, H. Basaran, J. A. Jackson, S. Kara, and M. Simsek (1995), High resolution seismic reflection profiling in the Sea of Marmara (northwest Turkey): Late Quaternary sedimentation and sea level changes, *Geol. Soc. of Am. Bull.*, *107*, 923–936.

Somoza, L., et al. (2003), Seabed morphology and hydrocarbon seepage in the Gulf of Cadiz mud volcano area: Acoustic imagery, multibeam and ultra-high resolution seismic data, *Mar. Geol.*, *195*, 153–176.

Stein, R. S., G. C. P. King, and J. Lin (1994), Stress triggering of the 1 994 *M* = 6.7 Northridge, California, earthquake by its predecessors, *Science*, *265*, 1432–1435.

Stein, R. S., J. H. Dieterich, and A. A. Barka (1996), Role of stress triggering in earthquake migration on the North Anatolian Fault, *Phys. Chem. Earth*, *21*, 225–230.

Stein, R. S., A. A. Barka, and J. H. Dieterich (1997), Progressive failure on the North Anatolian Fault since 1939 by earthquake stress triggering, *Geophys. J. Int.*, *128*, 594–604.

Stirling, C. H., T. M. Esat, K. Lambeck, and M. T. McCulloch (1998), Timing and duration of the last interglacial: Evidence for a restricted interval of widespread coral reef growth, *Earth Planet. Sci. Lett.*, *160*, 745–762.

Sylvester, A. G. (1988), Strike-slip faults, *Geol. Soc. Am. Bull.*, *100*, 1666–1703.

Tchalenko, J. (1970), Similarities between shear zones of different magnitudes, *Geol. Soc. Am. Bull.*, *81*, 1625–1640.

Thunell, R. C., E. Tappa, R. J. Varela, M. Llano, Y. Astor, F. E. Muller-Karger, and R. Bohrer (1999), Increased marine sediment suspension and fluxes following an earthquake, *Nature*, *398*, 233–236.

Toksöz, M. N., A. F. Shakal, and A. J. Michael (1979), Space-time migration of earthquakes along the North Anatolian Fault zone and seismicity gaps, *Pure Appl. Geophys.*, *117*, 1258–1270.

Wessel, P., and W. H. F. Smith (1998), New improved version of Genetic Mapping Tools released, *Eos Trans. AGU*, *79*, 579.

Witter, R. C., W. R. Lettis, J. Bachhuber, A. A. Barka, E. Evren, Z. Çakir, W. D. Page, J. Hengesh, and G. Seitz (2000), Paleoseismic trenching study across the Yalova segment of the North Anatolian Fault, Hersek peninsula, Turkey, in *The 1999 Izmit and Düzce Earthquakes: Preliminary Results*, edited by A. A. Barka et al., pp. 329–339, Istanbul Tech. Univ., Istanbul, Turkey.

Wong, H. K., T. Lüdmann, A. Ulug, and N. Görür (1995), The Sea of Marmara: A plate boundary sea in an escape tectonic regime, *Tectonophysics*, *244*, 231–250.

Wright, T. J., E. J. Fielding, and B. Parsons (2001), Triggered slip: Observations of the 17 August 1999 Izmit (Turkey) earthquake using radar interferometry, *Geophys. Res. Lett.*, *28*, 1079–1082.

E. Bonatti, G. Bortoluzzi, L. Gasperini, and A. Polonia, Institute of Marine Sciences, CNR, via Gobetti 101, Bologna I-40129, Italy.

N. Çagatay and N. Görür, Istanbul Technical University, Ayazaga, Istanbul 80626, Turkey.

M.-H. Cormier, C. M. G. McHugh, K. R. Newman, W. B. F. Ryan, and L. Seeber, Lamont-Doherty Earth Observatory of Columbia University, Palisades, NY 10964, USA. (cormier@ldeo.columbia.edu)

Ö. Emre, General Directorate of Mineral Research and Exploration, Ankara 06520, Turkey.